THE GEOLOGICAL SOCIETY OF AMERICA®

Bhumichula plateau: A remnant high-elevation low-relief surface in the Himalayan thrust belt of western Nepal

Tshering Z.L. Sherpa[1,†], Peter G. DeCelles[1], Barbara Carrapa[1], Lindsay M. Schoenbohm[2], and Joshua Wolpert[2]
[1]*Department of Geosciences, University of Arizona, Tucson, Arizona 85721, USA*
[2]*Department of Earth Sciences, University of Toronto, Toronto, Ontario M5S 3B1, Canada*

ABSTRACT

The Himalaya is known for dramatically rugged landscapes including the highest mountains in the world. However, there is a limited understanding of the timing of attainment of high elevation and relief formation, especially in the Nepalese Himalaya. Anomalous high-elevation low-relief (HELR) surfaces, which exhibit geomorphic antiquity and are possibly remnants of formerly widespread high-elevation paleosurfaces, provide a unique opportunity to assess the attainment of regional high elevation in the Himalaya. The Bhumichula plateau is one such HELR surface (4300–4800 m) in the western Nepalese Himalayan fold-thrust belt. The Bhumichula plateau is situated in the Dadeldhura klippe (also called the Karnali klippe), an outlier of Greater Himalayan Sequence high-grade metasedimentary/igneous rocks surrounded by structurally underlying Lesser Himalayan Sequence low-grade metasedimentary rocks. We assess the origin of the Bhumichula plateau by combining regional geological relationships and zircon and apatite (U-Th-Sm)/He and apatite fission track thermochronologic ages. The HELR surface truncates pervasive west-southwestward dipping foliations, indicating that it post-dates tilting of rocks in the hanging wall of the Main Central thrust above the Lesser Himalayan duplex. This suggests that the surface originated at high elevation by erosional beveling of thickened, uplifted crust. Exhumation through the ~180–60 °C thermal window occurred during middle Miocene for samples on the plateau and between middle and late Miocene for rocks along the Tila River, which bounds the north flank of the Bhumichula plateau. Cooling ages along the Tila River are consistent with erosional exhumation generated by early Miocene emplacement of the Main Central (Dadeldhura) thrust sheet, middle Miocene Ramgarh thrust emplacement, and late Miocene growth of the Lesser Himalayan duplex. The most recent middle-late Miocene exhumation took place as the Tila River and its northward flowing tributaries incised upstream, such that the Bhumichula plateau is a remnant of a more extensive HELR paleolandscape. Alpine glaciation lowered relief on the Bhumichula surface, and surface preservation may owe to its relatively durable lithology, gentle structural relief, and elevation range that is above the rainier Lesser Himalaya.

INTRODUCTION

Approximately 60 million years ago, the last vestige of Mesozoic Neotethyan oceanic lithosphere north of India was subducted beneath Eurasia and the northern extremity of continental Greater India came into contact with rocks that mark the southern edge of the continental Asian tectonic plate (Garzanti et al., 1987; DeCelles et al., 2014; Hu et al., 2015; Orme et al., 2015; Ding et al., 2016), launching a series of events that would ultimately affect the Tibetan-Pamir Plateau and produce the Himalaya, which together form Earth's greatest region of orogenic topography. The Himalaya is a southward verging fold-thrust belt produced entirely since the onset of the India-Eurasia collision (Gansser, 1964; Valdiya, 1980; Searle et al., 1987; Hodges, 2000), whereas Tibet is a composite of previously collided and variably reactivated Gondwanide terranes and suture zones dating back to Triassic time (Murphy et al., 1997; Yin and Harrison, 2000; Kapp and DeCelles, 2019). In addition to their different geologic histories, Tibet and the Himalaya are topographically distinct. Over a horizontal distance of scarcely more than 100 km the Himalaya rises from ~150 m above sea-level (asl) along its southern flank to the highest elevations on Earth, including 10 of the planet's 14 summits higher than 8000 m asl. Local relief exceeds 6000 m and slopes are >30° (Fielding et al., 1994; Duncan et al., 2003). The Tibetan Plateau, on the other hand, has much lower slopes, maximum local relief of ~2000–2500 m, and numerous lakes ranging in size from small glacial cirque lakes to deep basins such as Nam Tso (Lake Nam) and Mapham Tso (Lake Manasarovar).

The topographic contrast between the Himalaya and the Tibetan Plateau owes in part to the strong precipitation gradient across the southern flank of the Himalaya, where up to ~6 m of mostly summer monsoon rain is produced by air masses rising up the Himalayan orographic barrier from the Bay of Bengal and Arabian Sea (Bookhagen and Burbank, 2010; Islam et al., 2010; Andermann et al., 2012; Bohlinger and Sorteberg, 2017). Southerly air masses passing into Tibet are thus depleted of moisture, leaving Tibet arid to semi-arid (Molnar et al., 2010; Clift and Webb, 2019). Perhaps the most significant result of this climatic difference is in terms of erosion: Tibet is characterized by internal drainage with very little detrital export, while the southern flank of the Himalaya is being eroded 10–100 times faster by rivers in deep fluvial gorges, wet-based alpine glaciers, and mass movements (e.g., Blythe et al., 2007; Robert et al., 2009, 2011; Burbank et al., 2012; Herman et al., 2013; Streule et al., 2012; Rohrmann et al., 2012; Carrapa et al., 2016; Roback et al., 2018; DeCelles and Carrapa, 2021; Jepson et al., 2021), generating the planet's largest detrital efflux (Métivier et al., 1999; Curray et al., 2002). Two more contrasting erosional regimes can hardly be imagined, yet they are directly juxtaposed along the ~2300 km length of the Himalaya.

In this paper we consider the question of how long the present morpho-tectonic situation has prevailed. High paleoelevations in Tibet are now documented from late Oligocene onward (e.g., Quade et al., 2011, 2020; Ingalls et al., 2018), but almost nothing is known about the development of elevation in the Himalaya over much of

†tsheringzls@email.arizona.edu.

GSA Bulletin;
published online 14 December 2022

https://doi.org/10.1130/B36481.1; 11 figures; 3 tables; 1 supplemental file.

the Eocene through Miocene. Low-temperature thermochronologic data from the Mt. Everest region demonstrate strongly asymmetric exhumation, with rapid exhumation south of the peak but relatively slow exhumation (~0.25 mm/yr) since at least ca. 16–12 Ma on the north side (Sakai et al., 2005; Wang et al., 2010; Streule et al., 2012; Thiede and Ehlers, 2013; Carrapa et al., 2016). Slow erosion on the north side of the mountain is consistent with stable isotope data generated from shear zone synkinematic micas on Mt. Everest, which support high elevations during the Miocene (Gébelin et al., 2013). The regional configuration of the Main Central thrust (MCT) sheet, which is the principal structural unit that composes Mt. Everest (Carosi et al., 1999; Searle et al., 2003; Jessup et al., 2006; Streule et al., 2012) and the high Himalaya (Schelling, 1992; Hodges, 2000), demonstrates that its southern edge has been irregularly eroded back from a position close to the present front of the Himalaya, exposing structural windows through the thrust sheet and stranding erosionally isolated klippen of Greater Himalayan rocks (Fig. 1; Schelling, 1992; Srivastava and Mitra, 1994; DeCelles et al., 2001, 2020; Gehrels et al., 2006; La Roche et al., 2018a, 2018b, 2018c). If the erosional situation at Mt. Everest is typical, we would expect that regional high elevation in Nepal was much more widespread immediately after emplacement of the MCT sheet during early Miocene time (e.g., Hodges et al., 1996; Kohn, 2014), and that areas of high elevation have diminished as the trace of the MCT has retreated northward (Carrapa et al., 2016) and large erosional windows have exposed the structurally underlying rocks of the Lesser Himalayan Sequence. In Sikkim, Bhutan, and parts of Arunachal Pradesh, Greater Himalayan rocks in the hanging wall of the MCT sheet lie at high elevations (>4 km), close to the modern thrust front. Therefore, in the eastern Himalaya, we see an example of the paleo-MCT sheet that has not been eroded as far northward as it has in the western Himalaya.

One way to test this hypothesis is to identify remnants of formerly widespread high elevation surfaces in the region south of the zone of highest modern elevation. These surfaces would be expected to have developed upon a Greater Himalayan substrate at moderate to high elevation (compared to surrounding more recently eroded areas), and to exhibit evidence of great geomorphic antiquity as well as very slow recent erosion, in contrast to rapidly eroding regions of the Lesser Himalayan Zone. In keeping with the morphology of high glaciated regions of southernmost Tibet (i.e., the north slope of the high Himalaya), these surfaces might also characteristically exhibit low relief (e.g., Buceta et al., 2020). Such high-elevation low-relief (HELR) surfaces have been reported in almost all active orogens (e.g., Epis and Chapin, 1975; Gubbels et al., 1993; Masek et al., 1994; Kennan et al., 1997; Fielding et al., 1994; Abbott et al., 1997; Widdowson, 1997; Phillips, 2002; Schoenbohm et al., 2004; Clark et al., 2006; Grujic et al., 2006; Schildgen et al., 2007; van der Beek et al., 2009; Calvet et al., 2015; Adams et al., 2016; Zapata et al., 2019), where they range from a few tens of km^2 to large topographic plateau-like areas such as Tibet (~2 × 10^6 km^2), and have mean elevations that range between ~2 km and ~5 km.

The Bhumichula plateau is one such HELR surface in western Nepal, with elevations of 4300–4800 m and average slopes <18°, lying entirely within the Dadeldhura klippe, an erosional outlier of the MCT sheet (Fig. 2).We present new apatite fission track (AFT), zircon (U-Th-Sm)/He (ZHe), and apatite (U-Th-Sm)/

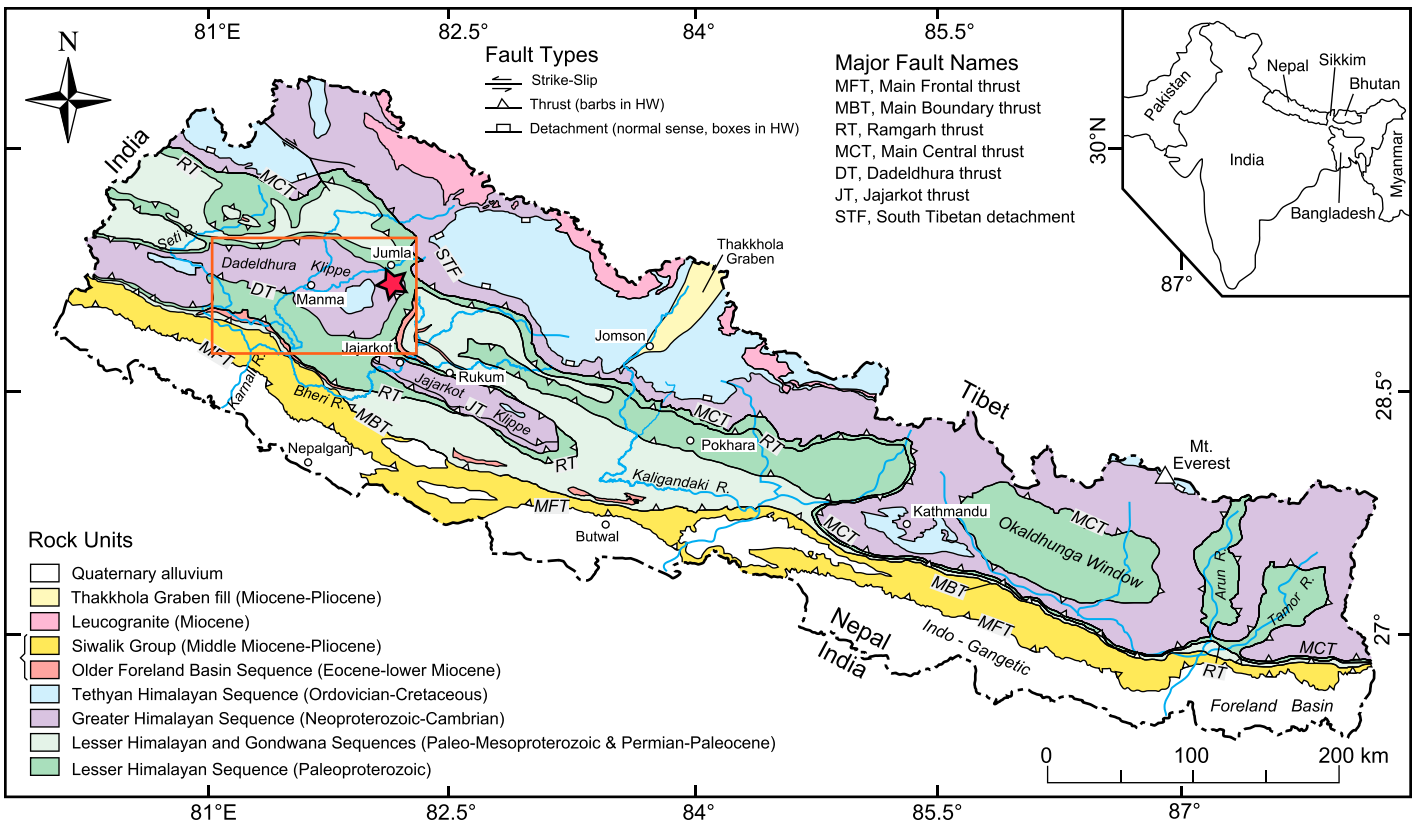

Figure 1. Geological map of Nepal (after DeCelles et al., 2020). Major rock units and regional fault systems are shown. Red rectangle outlines our study area in the Dadeldhura klippe. Red star denotes the Bhumichula plateau in the northeast limb of the Dadeldhura klippe. Inset shows geographic location of Nepal between India and Tibet.

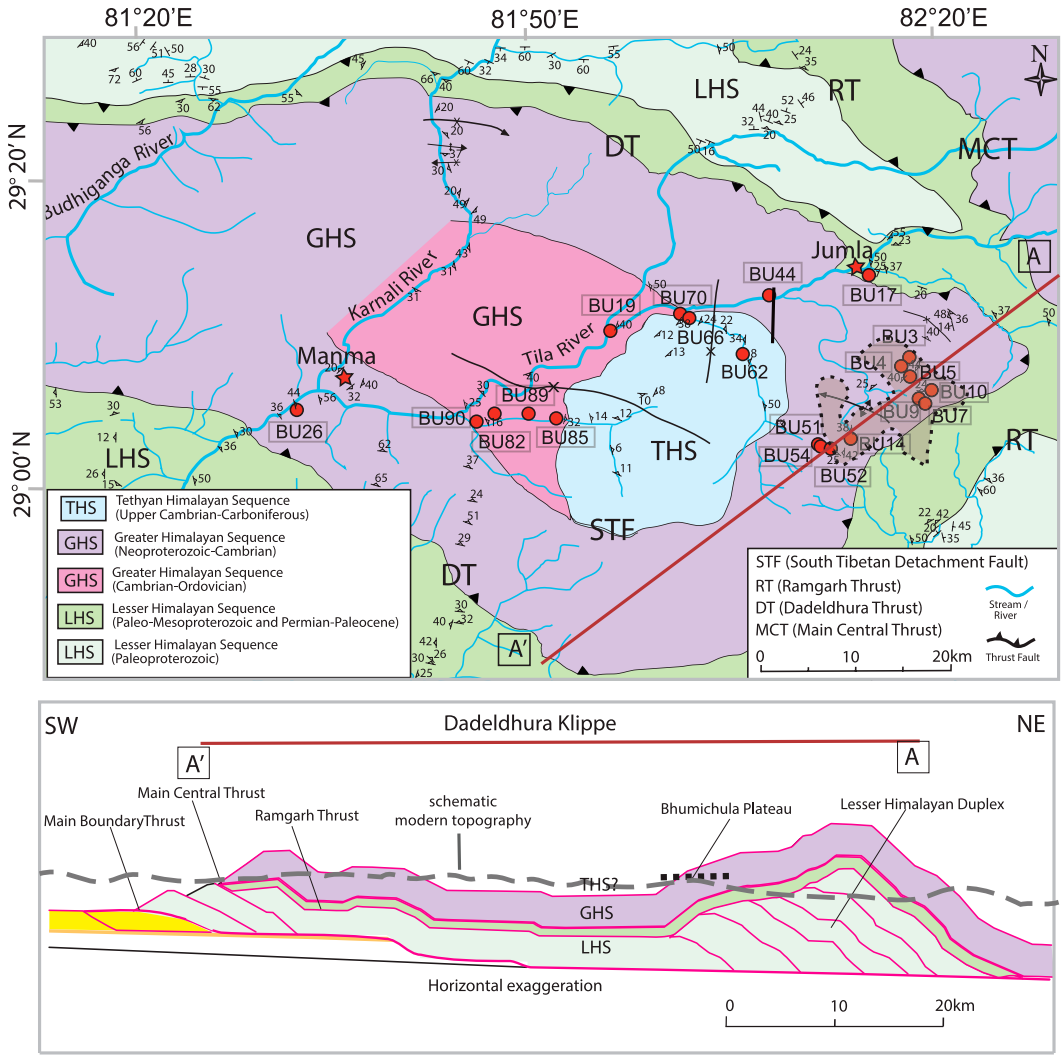

Figure 2. Enlarged geological map of the Dadeldhura klippe (after Soucy La Roche et al., 2016; DeCelles et al., 2020). Labeled red circles show locations of samples used for thermochronology in this study. Samples span the Bhumichula plateau and its flanks along the Tila and Karnali River valleys. Red stars indicate two major towns, Manma and Jumla. Dotted line encloses the Bhumichula plateau upstream of tributaries of the Tila River (northeast) and Bheri River (south). Lower panel shows northeast-southwest cross-section of Dadeldhura klippe (modified from DeCelles et al., 2020). Bhumichula high-elevation low-relief surface crosscuts west- to southwest-dipping foliation and lithologic contacts in the northeast limb of the klippe.

He (AHe) thermochronologic data as well as regional geological and geomorphological information to analyze the tectonic evolution and exhumation history of the Bhumichula plateau in western Nepal (Figs. 1 and 2). ZHe, AFT, and AHe systems are ideal for analyzing spatio-temporal patterns in near-surface exhumation because they have approximate closure temperatures of ~180 °C (Reiners, 2005), ~120 °C (Gleadow, 1981, 1986; Green et al., 1985) and ~60 °C (Ehlers and Farley, 2003), respectively, depending on cooling rates (Reiners and Brandon, 2006), and thus can resolve the exhumation history of rocks through a depth range of ~7–2 km in the upper crust (assuming a geothermal gradient of 25 °C/km). The structural setting of the Bhumichula plateau allows its development to be constrained within the temporal context of the kinematic history of the Himalayan thrust belt, which in turn facilitates a general paleogeomorphic reconstruction of this part of the Himalaya.

The Bhumichula Plateau: A HELR Surface in Western Nepal

Morphologically, we identify HELR surfaces in the Himalaya and Tibet as broad externally or partially internally drained regions, with elevations greater than 3800 m and average slopes less than 18° (van der Beek et al., 2009; Wilke et al., 2012). In Nepal and adjacent Tibet, HELR landscapes are widespread in the northern half of the Himalayan thrust belt—the Greater and Tibetan (or Tethyan) Himalayan zones, a region that transitions geomorphologically into the Tibetan Plateau (Buceta et al., 2020). This region is characterized by elevations ranging between ~4000 m and 8000 m, moderate to very high relief, alpine glaciers and associated landforms, and numerous lakes ranging in size from hundreds of m^2 to hundreds of km^2. In contrast, the southern part of the Himalayan thrust belt (referred to as the Lesser Himalayan Zone) has elevations ranging between ~500 m and 5000 m, is dominated by deep fluvial canyons, and has moderate to high relief. Lakes and glacial features are exceptionally rare, largely because of the predominance of steep fluvial geomorphology. In the Jumla district of western Nepal, however, an area of ~250 km^2 flanked on the north by the west-southwestward flowing Tila River and on the south by southeastward flowing tributaries of the Bheri River (Fig. 2) appears to be unique in that it lies far south of the region in which HELR surfaces are common and large (Buceta et al., 2020), and yet it exhibits all the characteristics of typical HELR surfaces, including small lakes, an average elevation of ~4500 m, low (~200–400 m) relief, and widespread glacial landforms (Figs. 3 and 4). We refer to this area as the Bhumichula plateau. This small region is morphologically similar to other, much larger, well-documented, HELR landscapes in the southeastern Tibetan Plateau (e.g., Clark et al., 2006) and well documented HELR surfaces in Pakistan, Sikkim, Bhutan,

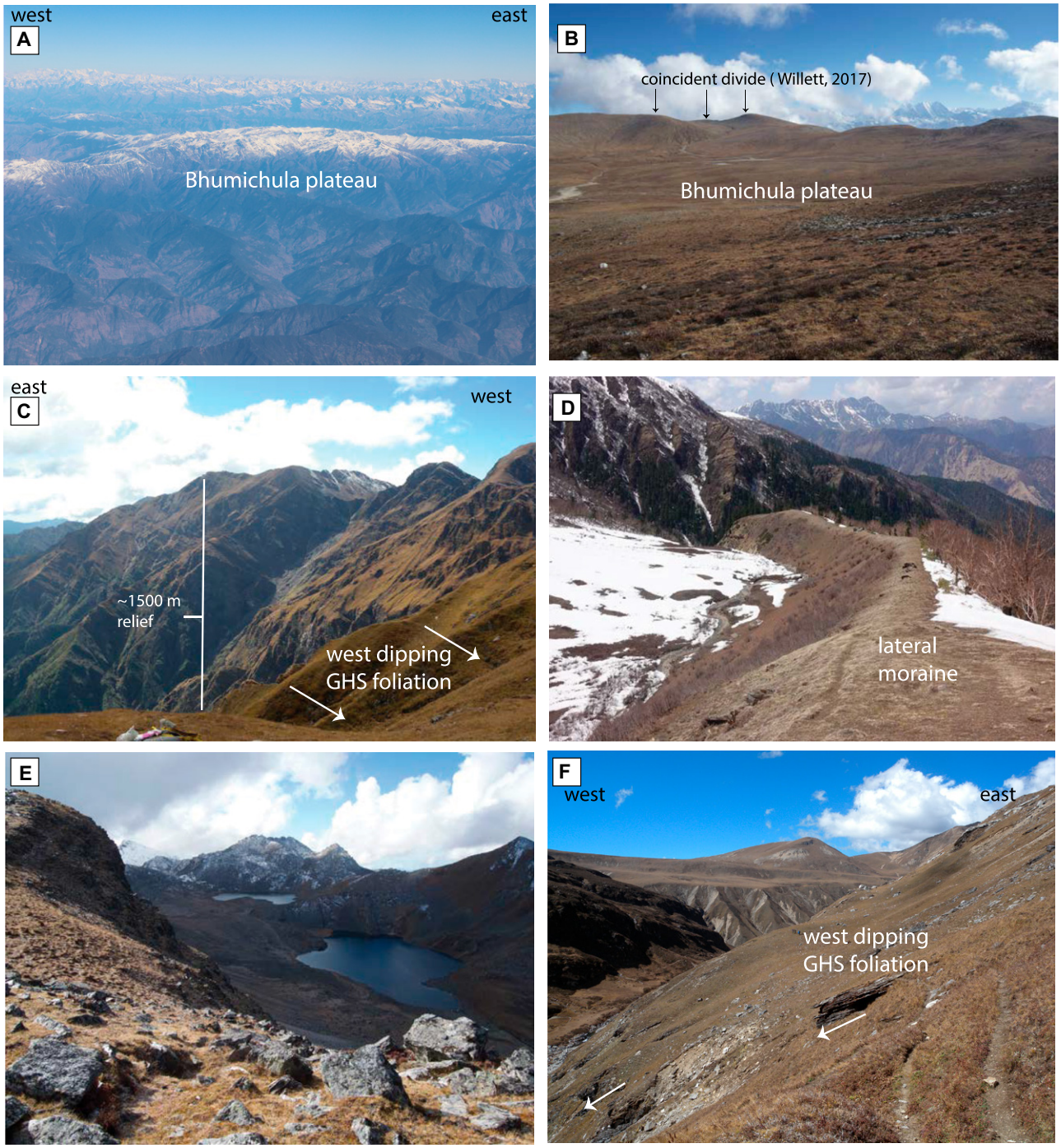

Figure 3. (A) Oblique low-elevation aerial photograph of the Bhumichula plateau from the southeast after a January snowstorm, with deep fluvial canyons in the Bheri River system in the foreground and high peaks of the Kanjiroba and Saipal Himals in the background. (B) Photograph taken on the Bhumichula plateau surface. The subdued topography on the plateau sharply contrasts with rugged topography of the High Himalaya (e.g., Kasi Dalpha, 6386 m; and Kanjiroba Himal, 6883 m) in the background. Low grassy ridge in middle ground is a coincident divide (Willett, 2017) along the northeastern edge of the plateau. (C) View southwest of southeastern flank of the Bhumichula plateau, which is incised by deep fluvial gorges and rugged topography (~1500 m of relief in this view) typical of parts of the Lesser Himalaya. Also visible is the pervasive west- and southwest-dipping (to the right in photo) foliation in Greater Himalayan Sequence (GHS) rocks that form the plateau. The plateau surface is out of view to the upper right. (D) View west of lateral moraine descending the southwestern flank of the Bhumichula plateau. (E) View south of two lakes (at 4435 m and 4487 m) in glacial cirques on the Bhumichula plateau. (F) View northward of west-dipping foliation in Greater Himalayan metasedimentary rocks (leftward dipping fabric highlighted by arrows in foreground), mantled by colluvium and buried by thick fill-terrace deposits in upper left.

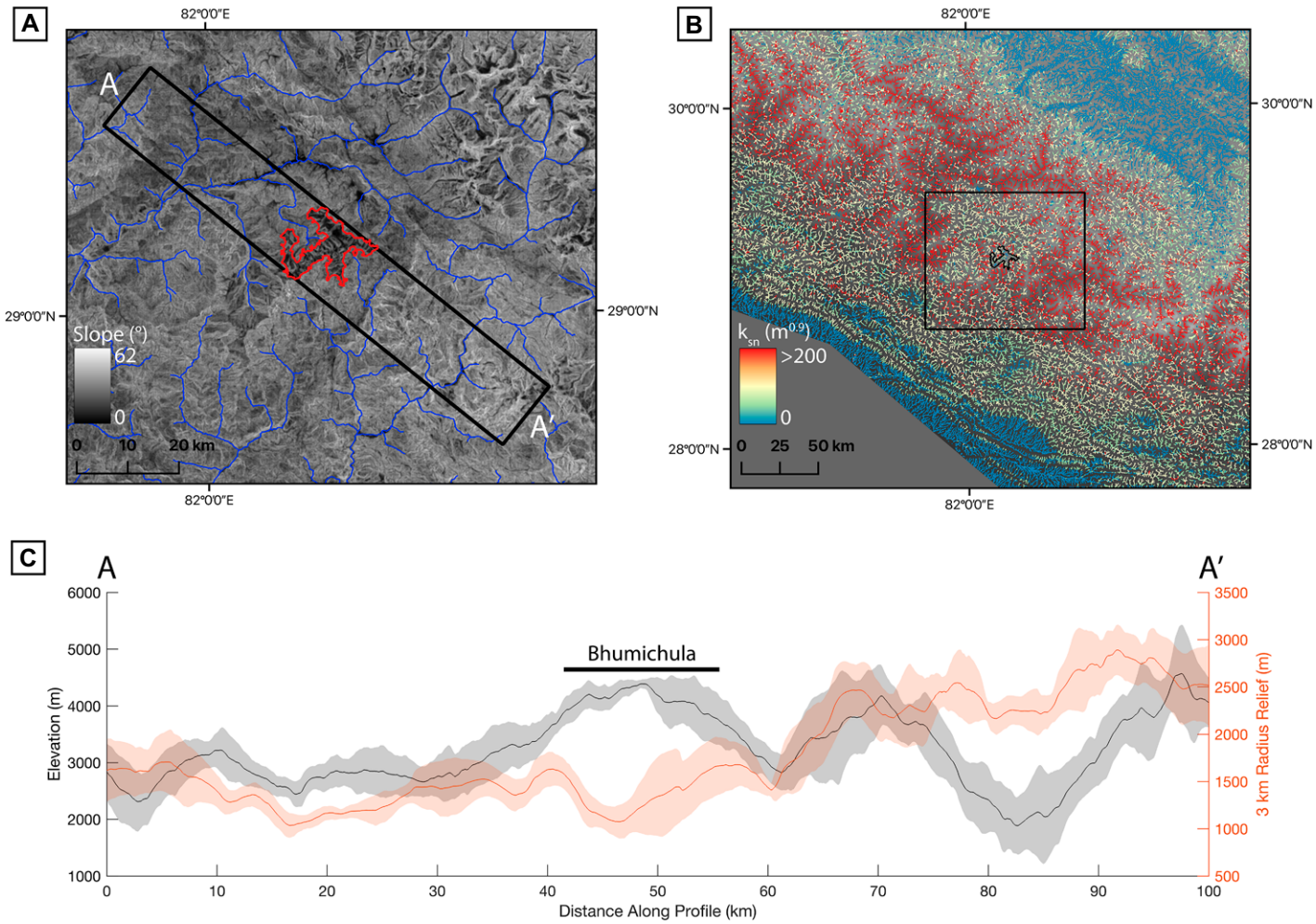

Figure 4. (A) Map of steepest slope averaged over 11 × 11 pixel windows on a 30 m resolution DEM. Rivers are colored blue whereas the Bhumichula plateau is outlined in red. Topography within the black rectangle was used to create panel C. (B) ksn measured with a reference concavity of 0.45. The large black box is the area shown in panel A with the Bhumichula plateau outlined in black. (C) Elevation and 3-km-radius relief swath profiles. The dark lines are averages along the length from A–A' in panel A, and the shaded regions are one standard deviation. DEM analyses were performed with TopoToolbox (Schwanghart and Scherler, 2014) and Topographic Analysis Kit (Forte and Whipple, 2019). The Bhumichula plateau's outline is defined by a region with <600 m relief over a 1 km radius and slopes <20°.

and Arunachal Pradesh (Grujic et al., 2006; van der Beek et al., 2009; Adams et al., 2015, 2016; Simoes et al., 2021).

The subdued topography of the Bhumichula plateau (Figs. 3A and 3B) contrasts with the surrounding high relief (>2 km), lower elevation landscape with average slopes >30° (Figs. 3C and 4A). The region surrounding the Bhumichula plateau is intensely dissected by tributaries of the Tila, Karnali, and Bheri rivers. The Tila River joins the Karnali River within the Dadeldhura klippe south of the town of Manma, whereas the Bheri River joins the Karnali near its downstream end in the frontal part of the fold-thrust belt. The Bhumichula plateau is currently unglaciated and has no permanent snowfields, though numerous remnants of alpine glaciation such as lateral, recessional, and terminal moraines are present (Fig. 3D) above elevations of ~4200 m in cirques below the highest summits. Although the Bhumichula plateau is not internally drained, it contains >30 small alpine lakes (Fig. 3E). As mentioned above, lakes are a defining feature of HELR surfaces in the Nepalese Himalaya.

Topographic variation is also expressed by differences in k_{sn}, a normalized channel steepness metric derived from a power law relation between river channel slope and contributing drainage area (Fig. 4B; Hack, 1973; Flint, 1974; Howard and Kerby, 1983). In detachment-limited systems where fluvial erosion is limited by the rate of bedrock incision rather than sediment transport capacity, k_{sn} can be useful in revealing relative rock uplift rates because river slopes tend toward a steady-state between rock uplift and erosion (Kirby and Whipple, 2001). For example, Cannon et al. (2018) showed that high k_{sn} streams coincide with high topography in the western Nepalese Himalaya due to recent strain accumulation and rock uplift.

Regionally, k_{sn} and slope values are relatively low over large tracts of the Dadeldhura klippe (Harvey et al., 2015), but are lowest on the Bhumichula plateau and along major river valleys (Fig. 4B). Our k_{sn} map shows lowest values (k_{sn} <200) on the plateau surface and higher values (k_{sn} ≈300) both on the north and south sides of the plateau, consistent with the obvious plateau-like morphology of the surface (Fig. 4C). Here, lithological variations do not affect k_{sn} because the Dadeldhura klippe is

predominantly composed of relatively resistant (Cannon et al., 2018) high-grade Greater Himalayan Sequence metasedimentary and metaigneous rocks (mainly orthogneiss, paragneiss, calc-gneiss, and leucogranite). Low k_{sn} on the Bhumichula plateau in comparison to surrounding catchments therefore likely reflects contrasts in erosion rates. Also evident from the slope map and topographic cross-section (Figs. 4A and 4C) is the asymmetric shape of the plateau, with a very steep southeast flank and a relatively gently sloping northwest side.

Geologic Setting of the Dadeldhura Klippe and Bhumichula Plateau

The Dadeldhura klippe (also called the Karnali klippe) is a ~200 km long, ~60 km wide erosional outlier of Greater Himalayan Sequence rocks that extends into northwest India as the Almora klippe (Figs. 1 and 2; Valdiya, 1980; Srivastava and Mitra, 1994; DeCelles et al., 2001; Robinson et al., 2006; Mandal et al., 2019). The klippe is a broad synformal structure with a multistage kinematic history owing to MCT and Ramgarh thrust emplacement, followed by growth of the underlying Lesser Himalayan duplex, which structurally elevated the northern limb of the Dadeldhura synform (Fig. 2). Dadeldhura klippe rocks are an erosional remnant of the MCT sheet (Fig. 5; DeCelles et al., 2001, 2020; Gehrels et al., 2006b; He et al., 2016; Soucy La Roche et al., 2018a). Detrital zircon U-Pb ages suggest the presence of both Tethyan Himalayan and Greater Himalayan rocks in the klippe (Gehrels et al., 2006b; Soucy La Roche et al., 2018a; DeCelles et al., 2020). Rocks in the footwall of the Dadeldhura thrust comprise Lesser Himalayan phyllite, quartzite, and granitic orthogneiss, whereas the hanging wall includes garnet-mica schist, quartz tectonite, granitic orthogneiss, tourmaline- and two-mica-bearing leucogranite, kyanite-bearing paragneiss, and phlogopite- and pyroxene-bearing marble. This difference in lithology, with more durable higher-grade metamorphic rocks above and weaker rocks below the Dadeldhura thrust (MCT) (Cannon et al., 2018) is partly responsible for the higher elevation of the Dadeldhura klippe.

Recent monazite U-Th/Pb petrochronology studies show that Greater Himalayan Sequence amphibolite facies rocks in the Dadeldhura klippe underwent prograde metamorphism as early as ca. 40 Ma, experiencing peak metamorphic conditions at ca. 36–30 Ma, and retrograde conditions at ca. 18 Ma (Braden et al., 2017). White mica $^{40}Ar/^{39}Ar$ cooling ages of ca. 18–22 Ma (DeCelles et al., 2001; Soucy La Roche et al., 2016), U-Th/Pb monazite ages for retrograde metamorphism ca. 11–8 Ma (Braden et al., 2017, 2018), and ZHe ages of ca. 14–9 Ma (DeCelles et al., 2020) in the northeastern part of the klippe also indicate that Dadeldhura rocks had started to cool below 450–475 °C by early Miocene and continued cooling through middle Miocene time. Apatite fission track (AFT) cooling ages of ca. 6–9 Ma have also been reported for rocks in the klippe (van der Beek et al., 2016; DeCelles et al., 2020). $^{40}Ar/^{39}Ar$ white mica cooling ages of ca. 15 Ma and AFT ages of ca. 8 Ma have been reported from modern sand samples along the Karnali River (van der Beek et al., 2016; Copeland, 2015). The range of early Miocene cooling ages reflects exhumation due to slip on the MCT, whereas middle-late Miocene cooling ages suggest Ramgarh thrust emplacement and subsequent passive uplift and erosion of overlying Greater Himalayan rocks as the Lesser Himalayan duplex developed (Fig. 5; Soucy La Roche et al., 2018a; DeCelles et al., 2020). Neither our mapping nor that of previous workers has documented significant high-angle faults cutting the northeastern part of the Dadeldhura klippe.

Hypotheses for Plateau Formation

The development of a HELR landscape like the Bhumichula plateau requires tectonic forcing for attainment of high elevation and a geomorphic mechanism for low relief formation. We will first address exhumation and rock uplift scenarios and then examine possible mechanisms that lead to relief reduction.

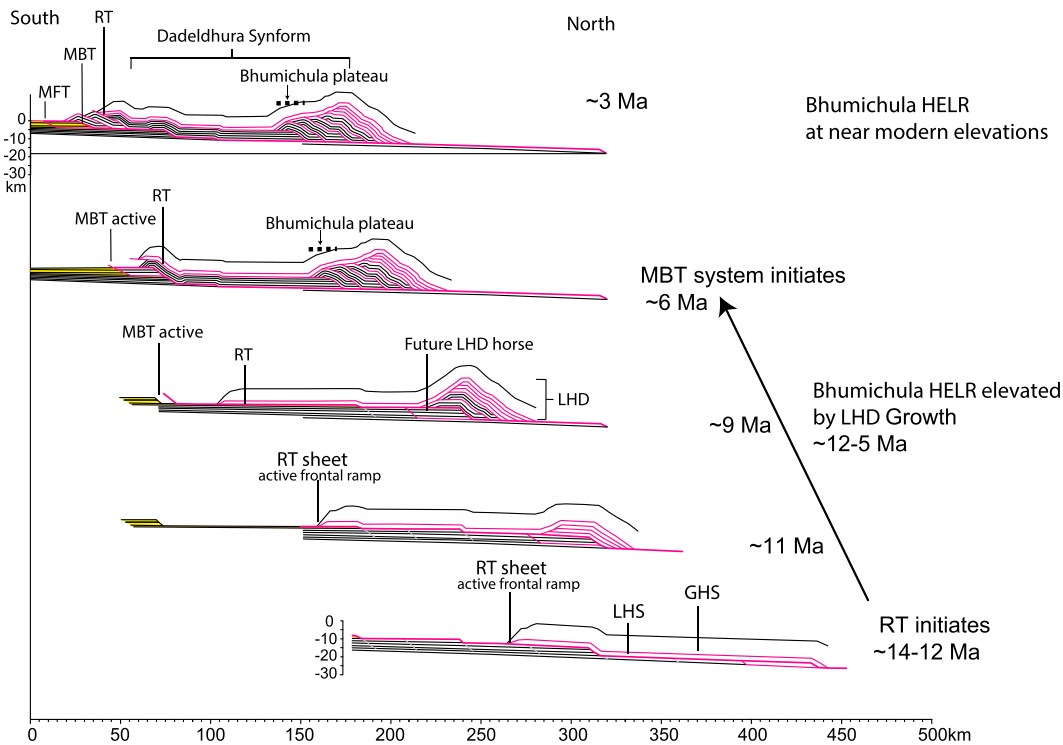

Figure 5. Partial kinematic sequence of thrusting events in the study area of western Nepal from balanced cross-sections (after DeCelles et al., 2020). Kinematic sequence shows emplacement of the Ramgarh thrust (RT), growth of the Lesser Himalayan duplex (LHD), and emplacement of the Main Boundary thrust (MBT) sheet. The Bhumichula plateau, shown by bold dashed line, formed during the last two stages of this reconstruction, after the main phase of growth of the LHD. Other abbreviations: GHS—Greater Himalayan Sequence; LHS—Lesser Himalayan Sequence; HELR—high-elevation low-relief. The *x*-axis represents horizontal distance north of a reference point just south of the Main Frontal thrust, and provides the scale of horizontal shortening during this time interval.

Exhumation and Rock Uplift Mechanism

Three hypothetical sequences of events can be considered for the exhumation history at the Bhumichula plateau:

(1) A low-relief landscape was formed at low elevation and was subsequently raised to high elevation (e.g., Clark et al., 2005; Whipple et al., 2017a). This would produce upstream propagating knickpoints and perhaps divide migration. The migrating knickpoints would cause upstream younging of cooling ages. Thermochronological ages would decrease with increasing elevation along the drainage network. Hypothesis (1) requires the Bhumichula plateau to predate any structural growth (Fig. 6).

(2) The plateau is a remnant of an extensive paleolandscape that formed as it rose to high elevations during crustal thickening. As the plateau uplifted, erosion along an antecedent river kept pace with uplift. In this scenario we expect thermochronological ages to remain quasi-constant along the main river, due to quasi-synchronous erosion along the main river, but they should generally increase with increasing elevation producing a "classic" age versus elevation profile (Fitzgerald and Stump, 1995) (Fig. 6).

(3) The plateau formed by crustal thickening-induced surface uplift, and rivers incised into the elevated region by knickpoint migration and/or headward erosion. Hypothesis (3) is similar to Hypothesis (2), but here we suggest that incision initiates downstream and progresses upstream leading to plateau isolation. This erosional mechanism predicts cooling ages that decrease upstream through the drainage network, such that ages at higher elevations are younger. Unlike Hypothesis

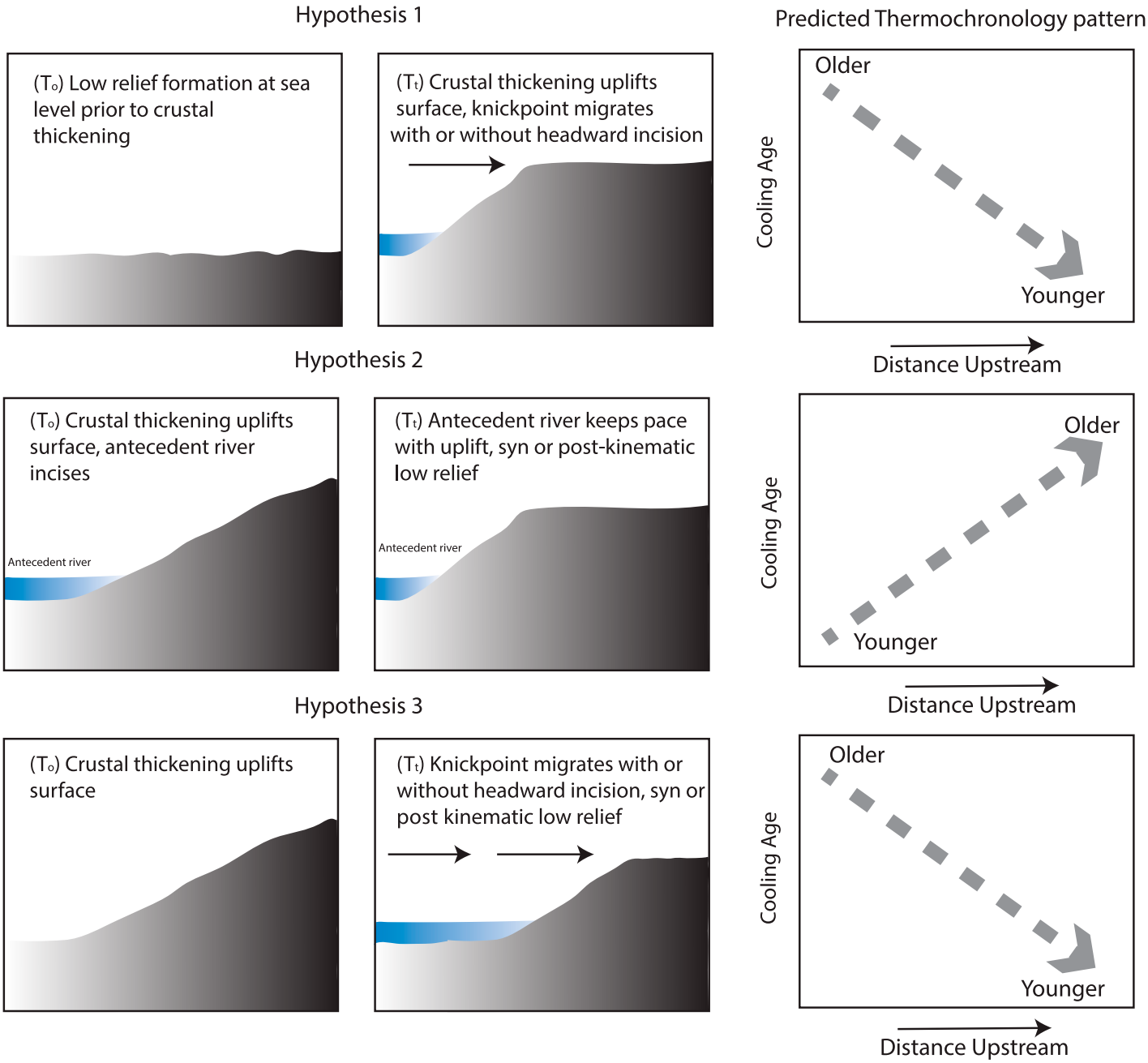

Figure 6. Cartoons illustrating the three hypotheses for development of the Bhumichula plateau and hypothetical thermochronologic patterns. T_o indicates time at initial step of development of the plateau and T_t indicates time after development of plateau.

(1) which suggests that the Bhumichula plateau is a prekinematic feature, Hypothesis (3) suggests that the Bhumichula plateau is either a synkinematic or postkinematic landscape (Fig. 6).

Low-Relief Development Mechanism

Any explanation for the Bhumichula plateau requires a mechanism for forming low relief, whether that low relief forms during or after attainment of high elevations in the region of the modern plateau. Low relief could form in situ at high elevations as a result of drainage area loss due to drainage basin reorganization (Willett et al., 2014; Yang et al., 2015; Willett, 2017). Early-middle Miocene uplift during Main Central and Ramgarh thrusting could have disrupted river drainage networks, causing incision and divide migration. As a divide migrates, an expanding drainage basin takes over the drainage area of a shrinking basin. The loss of discharge and erosional tools reduces erosion rates in the shrinking basin's trunk stream and causes relative surface uplift (rock uplift rate > erosion rate), which propagates upstream and progressively reduces relief in lower order catchments (in this case, the Bhumichula plateau; Yang et al., 2015; Whipple et al., 2017a). The effectiveness of this method for forming low relief surfaces depends on the response time of a trunk stream to drainage area loss and the frequency and magnitude of drainage area loss events (Whipple et al., 2017a and 2017b). From a thermochronological standpoint, samples from the plateau should yield late Miocene cooling ages reflecting the last regional tectonic event (duplex growth) that forced drainage reorganization and stream capture. Thermochronologic cooling ages are not expected to show a systematic spatial pattern but samples from the headwaters of expanding catchments on the exterior of the plateau should be younger than ages on the plateau. This hypothesis also predicts that sediment export from the plateau should be reduced as plateau-draining rivers suffer the effects of stream piracy and resulting loss of discharge; this could be manifest by young (Plio-Quaternary) sediment accumulations and fill terraces (Yang et al., 2015), as well as asymmetric drainage divides along plateau flanks (also referred to as coincident divides by Willett, 2017) where expanding drainages are juxtaposed with shrinking drainages (Whipple et al., 2017a; Willett, 2017).

The other obvious culprit that could drive the formation of low relief is alpine glaciation (Brozović et al., 1997; Shuster et al., 2011; Egholm et al., 2009; Zhang et al., 2016; Robl et al., 2020; Buceta et al., 2020), which has the ability to bevel the landscape at high elevation and prevent deep fluvial erosion. Given the abundance of glacial features on the Bhumichula plateau, we consider the role of glaciation in creation and preservation of low relief on the Bhumichula plateau later in this paper. In the northwestern Himalaya, extensive glaciation during the Quaternary is thought to have resulted in HELR surfaces (Brozović et al., 1997). If the Bhumichula HELR surface has experienced similar relief reduction due to glaciation, we might expect very young Quaternary cooling dates, but the very low-temperature range of such cooling might not be recorded in our lowest temperature thermochronologic systems.

SAMPLES, METHODS, AND RESULTS

Apatite Fission Track (AFT) Thermochronology

Fission tracks are the result of crystal lattice damage produced by spontaneous fission of ^{238}U; fission tracks are retained in apatite crystals at closure temperatures (T_c) below ~110 °C (Green et al., 1985) depending on cooling rates (Reiners and Brandon, 2006). Fission tracks can be healed in the partial annealing zone (PAZ) (Naeser, 1967; Gleadow and Duddy, 1981) which is considered to range between ~80 °C and ~120 °C (Naeser, 1967; Gleadow and Duddy, 1981; Green et al., 1985; Gallagher et al., 1998; Ketcham et al., 1999). Various studies have shown that rates of annealing also depend on individual grain chemistry (chlorine content) and crystallographic orientation of tracks along with temperature or the cooling rate (Barbarand et al., 2003; Donelick et al., 1999) and etching procedures (Murrell et al., 2009).

Zircon and apatite grains were separated from bulk samples by standard techniques involving crushing, sieving, and magnetic and heavy liquid separation. Apatite mineral separates were mounted in epoxy, polished, and etched using 5.5 mol HNO_3 at 21 °C for 20 seconds (Donelick et al., 2005). We used the external detector method (EDM) in which the density of counted spontaneous and induced fission tracks is combined with the ^{238}U decay constant and zeta calibration factor (Hurford and Green, 1983) to provide the time since the apatite crystal/grain passed through its closure temperature and accumulated spontaneous tracks. A thin, low-uranium mica sheet is used as an external detector that is attached to the mounted and etched sample before irradiation at Oregon State University (Corvallis, USA). A nominal fluence of 1.2×10^{16} n cm^{-2} was used at the reactor. After irradiation, mica sheets were etched with 40% HF for 45 min (Ketcham et al., 2007; Murrell et al., 2009). Approximately 20 apatite grains were counted per sample using the EDM method in the University of Arizona Fission Track Lab (Tucson, USA). We measured Dpar values for each sample (Table 2) as a proxy for apatite grain chemistry (Donelick et al., 2005). Confined track lengths are not reported due to lack of sufficient numbers in our samples. The chi-squared (χ^2) test for statistical homogeneity (Green, 1981) is used for all sample grain ages and all ages are reported as central ages. Raw counting data are reported in Tables 1 and 2 and Supplementary Table S1[1].

Apatite and Zircon (U-Th-Sm)/He Thermochronology

The (U-Th-Sm)/He age represents the time since a mineral has cooled through the T_c of ~60–70 °C for apatite (Farley, 2002; Ehlers and Farley, 2003) and 180–190 °C for zircon (Reiners 2005). At temperatures higher than T_c, ^4He diffuses out of the mineral domain. However, the switch from diffusion to retention is not instantaneous but occurs within a temperature range at which He is partially retained within the grain, called the partial retention zone (PRZ) (Wolf et al., 1996; Warnock et al., 1997; House et al., 2000; Ault et al., 2019). The PRZ temperature range is ~40–70 °C for the AHe system (Zeitler et al., 1987; Farley 2002) and ~165–195 °C for the ZHe system (Zeitler et al., 1987; Wolf et al., 1996; Warnock et al., 1997; Farley 2002; Ehlers and Farley 2003). Each grain could also have a unique cooling age variation (Fitzgerald et al., 2006) depending on radiation damage (Flowers et al., 2009), alpha particle ejection (Meesters and Dunai, 2002), grain size (Reiners and Farley, 2001), crystal chemistry (Gautheron et al., 2013), particle injection from neighboring minerals (Spiegel et al., 2009), mineral coatings (Murray et al., 2014), and lattice defects and zonation (Farley et al., 2011; Murray et al., 2014; Orme et al., 2015), which can add complexity to thermal histories.

In both AHe and ZHe systems, radiation damage affects retention of He (Shuster et al., 2006; Shuster and Farley 2009; Guenthner et al., 2013; Guenthner, 2020; Gautheron et al., 2019; Gérard

[1]Supplemental Material. Figure S1: Inverse thermal models generated for samples upstream on the Bhumichula plateau at elevations >4000 m. Figure S2: Inverse thermal models generated for samples downstream of Bhumichula plateau and its flanks at elevations <4000 m. Figure S3: Zircon Date-eU plots. Figure S4: Apatite Date-eU plots. Figure S5: Radial plots for AFT samples generated using Radial Plotter (Vermeesch, 2009). Table S1: Repository data of raw apatite fission track data. Table S2: Zircon (U-Th)/He. Table S3: Apatite (U-Th)/He. Table S4: Summary of inverse thermal modeling strategy and results. Please visit https://doi.org/10.1130/GSAB.S.21091264 to access the supplemental material, and contact editing@geosociety.org with any questions.

TABLE 1. SUMMARY OF APATITE FISSION TRACK (AFT), ZIRCON, AND APATITE U-Th/He AGES (ZHe, AHe)

Bedrock samples	Elevation (m)	Latitude (°N)	Longitude (°E)	Lithology	ZHe range (Ma)	AHe range (Ma)	AFT central ages (Ma)	1σ
Bhumichula plateau								
BU7*	4780	29.12138	82.26426	leucogranite	6.8 ± 0.1–14.3 ± 0.2		6.5	0.9
BU9*	4709	29.12356	82.26176	paragneiss		6.4 ± 0.1–7.1 ± 0.1	9.4	1.6
BU10	4581	29.13230	82.27167	leucogranite		5.4 ± 0.2–6.1 ± 0.1		
BU 5	4493	29.14887	82.25004	paragneiss		4.3 ± 0.2–5.4 ± 0.1		
BU4*	4400	29.16154	82.24099	paragneiss		6.9 ± 0.1–7.8 ± 0.1	8.8	1.9
BU14	4313	29.07807	82.18122	paragneiss			9.3	1.5
BU3*	4210	29.16972	82.24859	leucogranite	9.6 ± 0.1–13.5 ± 0.2		6.9	2.5
Bhumichula plateau flanks								
BU52*	4420	29.07082	82.15670	leucogranite		9.14 ± 0.1	9.9	1.9
BU54*	4126	29.07269	82.14843	leucogranite	9.6 ± 0.1–11.7 ± 0.2	4.6 ± 0.1–14.9 ± 0.4	10.3	2.0
BU51	4046	29.07265	82.14676	leucogranite			10.5	2.6
Along Tila River								
BU44*	3425	29.24079	82.09010	leucogranite	6.0 ± 0.1–6.5 ± 0.1	5.7 ± 0.1–8.41 ± 0.1	6.7	1.4
BU85*	2792	29.10409	81.85284	orthogneiss	8.8 ± 0.1–14.3 ± 0.2		9.1	1.6
BU17	2601	29.26511	82.20127	paragneiss	4.9 ± 0.1–6.1 ± 0.1			
BU62	2389	29.17472	82.06152	leucogranite			14.3	3.2
BU82*	2349	29.10552	81.82075	orthogneiss		3.72 ± 0.1–10.2 ± 0.1	12.4	3.1
BU66*	2241	29.21620	82.00261	leucogranite	8.2 ± 0.1–14.9 ± 0.2	6.5 ± 0.1–9.8 ± 0.1	10.7	2.7
BU70	2201	29.22047	81.9925	leucogranite	6.8 ± 0.1–9.7 ± 0.1			
BU19*	2055	29.20121	81.91278	orthogneiss	8.6 ± 0.1–10.1 ± 0.1		8.8	1.7
BU 89	2004	29.10567	81.78368	orthogneiss		8.6 ± 0.1–9.9 ± 0.1		
BU90*	1535	29.09839	81.76440	orthogneiss		7.2 ± 0.1–11.9 ± 0.2	14.9	3.8
BU26*	753	29.12056	81.55506	orthogneiss	11.1 ± 0.2–12.6 ± 0.2	5.4 ± 0.1–9.9 ± 0.1	10.7	1.5

*Samples used for thermal modeling.

et al., 2020) possibly due to interaction between alpha recoil, fission track damage zones, or other type of damage (Guenthner et al., 2013; Ketcham et al., 2013; Gautheron et al., 2019). Effective uranium concentration (eU = U + 0.235 × Th) is used as a proxy for radiation damage (Shuster et al., 2006; Flowers et al., 2007) and date-eU relationships are used to refine time-temperature paths by allowing analysis of apatites and zircons with wide variation in temperature sensitivities. If rocks reside in the PRZ long enough, apatites and zircons that have experienced the same thermal history will have positive date-eU relationships. In this case, apatite and zircons with higher eU experience higher radiation damage which reduces He diffusivity and results in higher closure temperatures or older dates (Nasdala et al., 2004; Shuster et al., 2006; Flowers et al., 2009; Guenthner et al., 2017; Recanati et al., 2017). However, after zircons pass a peak radiation damage threshold, He diffusion increases abruptly resulting in negative date-eU relationships (Nasdala et al., 2004; Reiners, 2005; Guenthner et al., 2013, 2014, 2017, 2020; Orme et al., 2016).

Four single-crystal aliquots were analyzed per sample for AHe and five single crystal aliquots were used for ZHe. Each grain was selected on the basis of morphology and size. Digital photomicrographs were used to record grain dimensions, which are used to correct for alpha ejection in all zircon and apatite crystals (Ketcham et al., 2011). Apatites and zircons were handpicked and placed in Nb tubes, which act as micro-furnaces and avoid volatilization of parent nuclides during laser heating. The tubes were heated with Nd:YAG and CO_2 laser beams up to 900–1000 °C for apatite and 900–1300 °C for zircon in an ultrahigh vacuum chamber to release helium (^{4}He) which is cryogenically purified and measured using a quadrupole mass spectrometer. U, Th, and Sm concentrations

TABLE 2. AFT DATA FROM THE BHUMICHULA PLATEAU SURFACE, FLANKS, AND ALONG TILA RIVER IN WESTERN NEPAL

Sample	ρ_d (10^6)	Nd	ρ_s (10^6)	Ns	ρ_i (10^6)	Ni	Central age (Ma)	Error (± 1σ)	ρ^2 (%)	No. of grains counted	D_{par}
Bhumichula surface											
BU7*	1.286	4321	0.10930	82	3.910	2933	6.50	0.9	100	19	1.6
BU9*	1.271	4321	0.22800	63	5.812	1606	9.39	1.6	31	13	1.3
BU4*	1.345	4321	0.10810	27	3.005	751	8.75	1.9	100	14	1.3
BU14	1.198	4321	0.15200	60	3.483	1375	9.34	1.5	100	19	1.3
BU3*	1.360	4321	0.04524	10	1.389	307	6.90	2.5	93	6	2.0
Bhumichula flanks											
BU52*	0.984	4181	0.09570	34	1.720	611	9.91	1.9	100	20	1.4
BU54*	1.040	4181	0.09288	33	1.697	603	10.30	2.0	100	20	1.5
BU51	0.927	4181	0.07076	20	1.136	321	10.45	2.6	100	17	1.5
Along Tila River											
BU44*	0.871	4181	0.11650	46	2.743	1083	6.70	1.4	100	20	1.5
BU85*	1.172	4181	0.10640	42	2.175	977	9.11	1.6	99	20	1.3
BU62	1.059	4181	0.09047	25	1.216	336	14.25	3.2	100	16	1.6
BU82*	1.153	4181	0.07794	20	1.286	330	12.43	3.1	100	15	1.4
BU66*	0.893	4024	0.00699	20	1.363	390	10.69	2.7	100	17	1.4
BU19*	1.032	4024	0.09515	37	2.019	785	8.80	1.7	100	19	1.7
BU90*	1.210	4181	0.06422	18	9.419	264	14.91	3.8	100	15	1.4
BU26*	1.124	4321	0.28010	94	5.329	1788	10.69	1.5	100	18	2.0

Note: TLS (Tshering Lama Sherpa) zeta: 362 ± 30.
*Samples used for thermal modeling.
AFT—apatite fission track.

TABLE 3. MODELING PARAMETERS FOR HeFTy INVERSE THERMAL MODELS GENERATED IN THIS STUDY FOLLOWING FLOWERS ET AL. (2015)

1. Thermochronological data for inverse modeling

AFT Data	Data Source	Parameters		
BU3	S1	2Ev		
BU4	S1	2Ev		
BU7	S1	2Ev		
BU9	S1	2Ev		
BU19	S1	2Ev		
BU52	S1	2Ev		
BU82	S1	2Ev		
BU85	S1	2Ev		
BU90	S1	2Ev		
ZHe Data	**Data Source**	**Parameters**	**Error applied for U-Th/He ages**	**No. of grains modeled**
BU3	S2	2Ev	30%	1,3,4,5
BU7	S2	2Ev	10%	1,2
BU19	S2	2Ev	20%	1,2,4,5
BU26	S2	2Ev	20%	1,3,5
BU44	S2	2Ev	20%	2,3,5
BU54	S2	2Ev	30%	2,3,5
BU66	S2	2Ev	30%	1,2,5
BU85	S2	2Ev	20%	1,3,4,5
AHe Data	**Data Source**	**Parameters**		**No. of grains modeled**
BU4	S3	2Ev	1s	2,4
BU9	S3	2Ev	10%	1,2,3
BU26	S3	2Ev	20%	1,2,3
BU44	S3	2Ev	20%	1,4
BU54	S4	2Ev	30%	1,2
BU52	S3	2Ev	1s	4
BU66	S3	2Ev	30%	1,4
BU82	S3	2Ev	10%	2,3
BU90	S3	2Ev	10%	1,4

Data treatment, uncertainties, and other relevant constraints
He data.
Aliquotes which showed a date-eU relationship (Figs. S3 and S4) were modeled to find at least 100 good paths.
He data treatment: Each zircon and apatite grain was modeled independently but simultaneously for each sample.
Error applied for U-Th/He ages: More details in Table S4 and Figures S1 and S2.
Uncorrected dates were corrected for alpha ejection and stopping distance using Ketcham et al. (2011) in HeFTy.
Alpha calculation: ejection.
Etching: 5.5 molar nitric acid (Ketcham et al., 2007).
Segment code used: 2Ev.
The number of times the segments between constraints are halved is 2 times (2).
Randomizer style is Episodic mode (E).
Paths between constraints is monotonic variable (v).
2. Additional geologic information
Samples are mostly early Miocene leucogranites or migmatites hosting leucogranites.
Soucy La Roche et al. (2018) show cooling through $^{40}Ar/^{39}Ar$ closure temperatures of 20–17 Ma in the southwest limb of the Dadeldhura klippe and 17–14 Ma in the northeast limb.
3. System and model specific parameters
ZHe Model: ZRDAAM, Guenthner et al. (2013).
AHe Model: RDAAM, Flowers et al. (2009).
FT annealing model: Ketcham et al. (2007).
FT c-axis projection: yes (Ketcham et al., 2007).
Statistically fitting criteria: standard HeFTy values number of paths attempted when number of good paths =100.
GOF: "good fit" 0.5, "acceptable fit" 0.05.
AFT—apatite fission track; ZHe—zircon (U-Th-Sm)/He; AHe—apatite (U-Th-Sm)/He (AHe).

are then measured by isotope dilution using an inductively coupled plasma mass spectrometer (Reiners and Nicolescu, 2006). Durango Apatites and Fish Canyon Tuff zircons are used as standards to check analytical procedures and calibrations for AHe and ZHe, respectively. All (U-Th-Sm)/He analyses were done at the University of Arizona Radiogenic Helium Dating Laboratory (Tucson, USA).

Thermal History Modeling

We used inverse modeling in HeFTy v1.9.3 to resolve time-temperature (t-T) paths for each rock sample (Ketcham, 2005; Vermeesch and Tian, 2014) using a combination of AFT, ZHe, and AHe cooling data. Inverse modeling in HeFTy searches thousands of random, independent t-T paths to report candidate thermal histories that match geological constraints and measured data to pass user-defined "good" and "acceptable" goodness of fits (Ketcham 2005; Ketcham, 2017).

One of the greatest utilities of thermal history modeling is the incorporation of several thermochronometers to constrain the cooling history of a single sample. Complimentary cooling ages from two thermochronologic systems can create a more accurate cooling history that can cover a wider temperature range than a single chronometer. We therefore only model samples from which we have cooling ages from at least two thermochronometers (Table 1; Figs. S1 and S2). For samples with all three thermochronometers, we use AHe and ZHe cooling ages for thermal modeling and AFT cooling ages to check the thermal history models. More details are provided in Table 3 and Supplementary Table 4. For samples with either AHe or ZHe data, we chose to model grains that followed a date-eU trend (Figs. S3 and S4).

Several studies have shown that overdispersion in AHe (Vermeesch, 2010; Stevens Goddard et al., 2018; Winn et al., 2017) and ZHe data (Ginster, 2018 ; Carrapa et al., 2019) is due to underestimation of system uncertainties that result in difficulty modeling t-T paths (Winn et al., 2017; Bhattacharya et al., 2020). AHe and ZHe systems are susceptible to error beyond analytical uncertainties that involve inaccuracies in treatment of either radiation damage annealing or corrections related to undetected microinclusions and alpha injection from neighboring minerals (Ginster, 2018; Stevens Goddard et al., 2018; Winn et al., 2017). To account for overdispersion and additional errors in the AHe and ZHe data, we increased uncertainties in AHe and ZHe (Table 3) for our models in HeFTy. The error for each grain is assigned to create enough variability to allow good paths in our thermal history models. We started each model with only the analytical error (1σ) and then increased the error in increments of 10% (Table S4) until we found acceptable and good paths (Figs. S1 and S2). The amount of grain error required was variable per grain, which we attribute to unknown analytical uncertainties associated with individual grains.

Date-eU trends (Figs. S3 and S4) were employed as a first-order check to select apatite and zircon grains that experienced similar thermal histories. We then modeled single grain ages separately (Table 3; Tables S2 and S3) using the RDAAM calibration model (Flowers et al., 2009) and the ZRDAAM calibration model (Guenthner et al., 2013). Annealing models from Ketcham et al. (2007) for AFT data and alpha ejection corrections from Ketcham et al. (2011) for (U-Th)/He data were used. Previous $^{40}Ar/^{39}Ar$ data (Soucy La Roche et al., 2018a) from the Dadeldhura synformal klippe show that rocks in the southwest limb of the synform cooled below 450–475 °C, ca. 20–17 Ma whereas the northeast part of the klippe cooled between ca. 17 and 14 Ma. Therefore, we placed an initial constraint on the modeling that required samples to be hotter than 300 °C (greater than the closure temperature of white mica $^{40}Ar/^{39}Ar$) between 25 and 14 Ma in the model. The models also constrained near-surface temperatures by 2–0 Ma to be consistent with geological observations. Additional input parameters are listed in Table 3 according to procedures outlined in Flowers et al. (2015). We refer to ZHe, AFT, and AHe data sets as "dates" when interpreted without geology, and as "ages" when interpreted in a regional geological context.

AFT, ZHe, and AHe Results

This study generated AFT, AHe, and ZHe data from samples distributed across the Bhumichula plateau surface and its flanks and along the Karnali and Tila rivers (Fig. 2). All 16 AFT samples passed the χ^2 test for homogeneity (Tables 1, 2). We report the central ages of each sample (Table 1) as well as the complete data set (Table 2; Table S1). ZHe and AFT dates generally overlap within error whereas AHe dates are younger (Tables 1 and 2).

Samples from the Dadeldhura klippe have middle-late Miocene cooling dates. Both AFT and ZHe dates are progressively younger northeastward along the Tila River above its confluence with the Karnali River (Figs. 7 and 8). Samples closer to the Karnali yield AFT dates between ca. 15 and ca. 10 Ma whereas samples on the Bhumichula plateau, farther upstream, exhibit AFT dates between ca. 9 and ca. 6.5 Ma (Table 1). The younging trend along the Tila River is reflected in ZHe dates as well, with ages decreasing from ca. 12 Ma to 6 Ma upstream from the Karnali-Tila confluence (Figs. 7 and 8; Table 1). AHe dates along the Tila River yield a range of cooling dates between ca. 9 Ma and 5 Ma, with no obvious spatial or elevation patterns (Figs. 7 and 8; Table 1).

AFT and ZHe date versus elevation trends also show younging dates with increasing elevation (Fig. 8). Our samples fall into two groups in terms of elevation: those that were collected up to ~3400 m elevation, and those that were collected from the plateau surface beginning ~4100 m elevation and continuing up to 4780 m (Fig. 8; Table 1). As elevation increases from ~1500 to ~3400 m, samples collected along the Tila River show AFT dates that decrease from ca. 15 Ma to 7 Ma, ZHe dates that decrease from ca. 12 to ca. 6 Ma, and AHe dates that decrease from ca. 9 to ca. 6 Ma. For samples above 4000 m at the edge of the plateau, AFT dates become abruptly older, up to ca. 10 Ma at ~4100 m, decreasing upward to ca. 6.5 Ma at ~4780 m. Similar patterns are evident in the ZHe and AHe dates, which decrease from ca. 12 Ma to ca. 6 Ma and ca. 9 Ma to ca. 6 Ma, respectively, from elevations of ~4000 m to ~4780 m (Table 1).

Although our inter-sample (U-Th-Sm)/He dates vary, AHe data fall into positive date-eU trends and ZHe data fall into positive or negative date-eU trends (Figs. S3 and S4) as expected due to radiation damage accumulation (Flowers et al., 2009; Guenthner et al., 2013).

Thermal History Modeling Results

Thirteen thermal models were generated for samples along the Tila River and its tributaries upstream of the Karnali-Tila confluence; these samples were collected from SW to NE upstream along the Tila River. The samples in upstream order, in terms of both distance from the Karnali confluence and elevation, are BU26, BU90, BU82, BU85, BU19, BU66, and BU44 along the Tila River, and BU54, BU52, BU3, BU4, B7, and BU9 on the Bhumichula plateau.

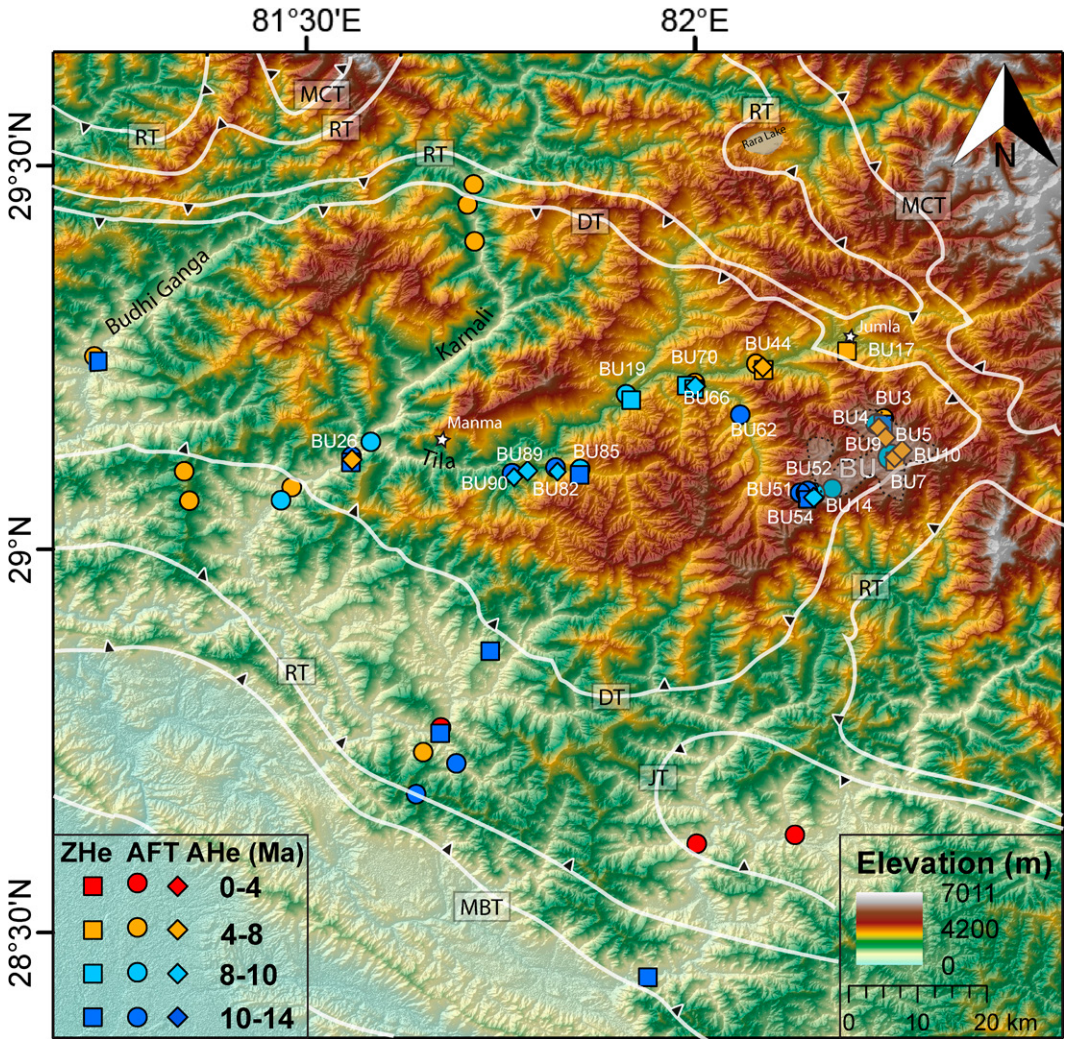

Figure 7. Digital elevation model showing low-temperature thermochronology from the Bhumichula plateau and the western Nepalese Himalaya (van der Beek et al., 2009; Sakai et al., 2013; DeCelles et al., 2020; this study). Thermochronology samples from this study along the Tila River and the Bhumichula high-elevation low-relief surface are labeled in white. Shaded area labeled BU—Bhumichula plateau; DT—Dadeldhura thrust; RT—Ramgarh Thrust; MCT—Main Central Thrust; MBT—Main Boundary Thrust. Major thrust faults are shown as white barbed lines, with barbs on the hanging wall. ZHe—zircon (U-Th-Sm)/He; AFT—apatite fission track; AHe—apatite (U-Th-Sm)/He.

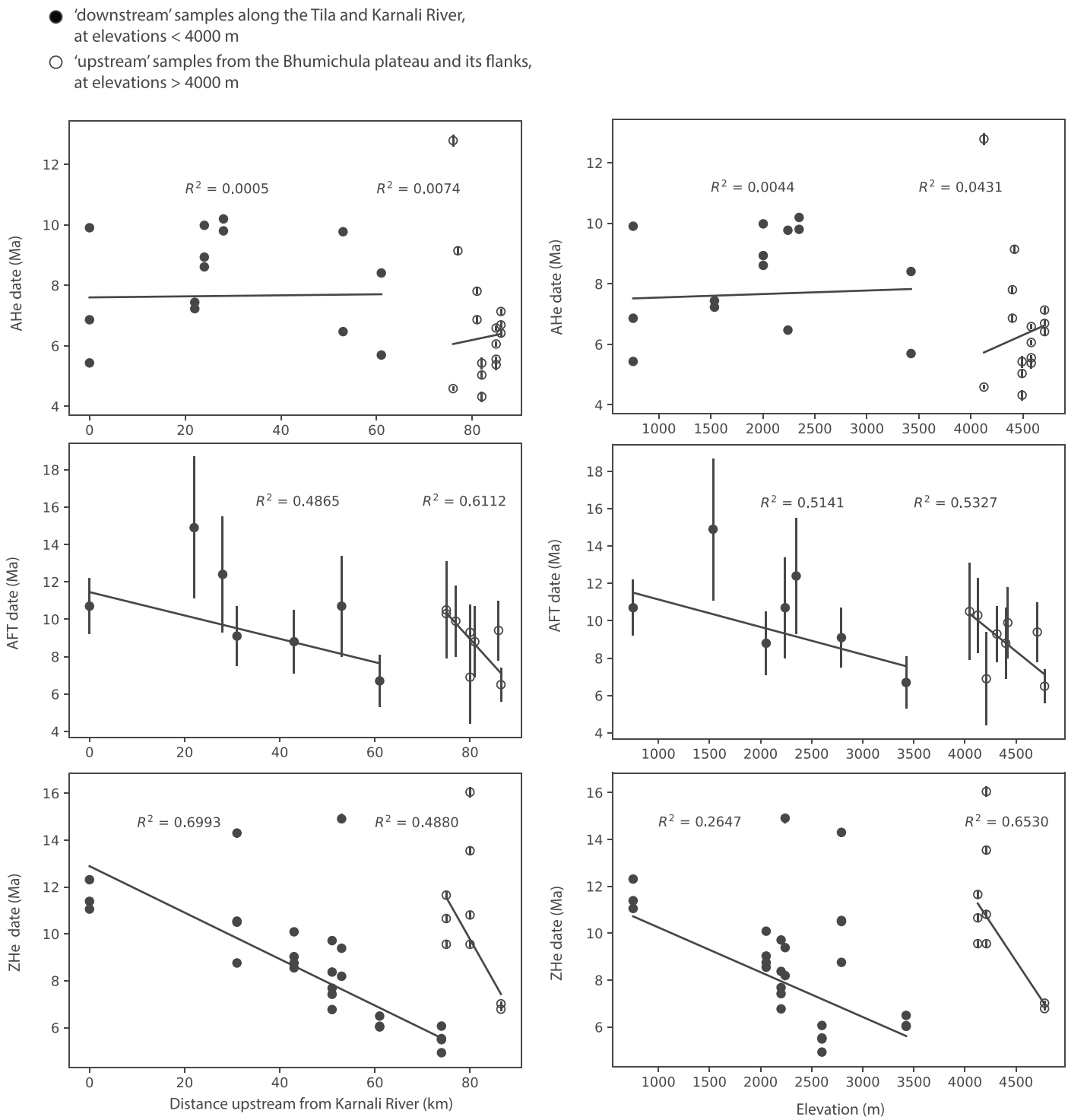

Figure 8. Graphs showing dates versus distance upstream from the Tila-Karnali confluence (left) and dates versus elevation (right) for apatite (U-Th-Sm)/He (AHe), apatite fission track (AFT), and zircon (U-Th-Sm)/He (ZHe) data sets (top, middle, and bottom, respectively). AHe, AFT, and ZHe dates are grouped to show upstream (open circles) and downstream (black filled circles) samples. All samples along the Tila River and Karnali River are downstream at low elevations (<4000 m). Samples on the Bhumichula plateau and its flanks are defined as upstream samples at high elevations (>4000 m). Black lines show linear weighted regressions through upstream and downstream data sets.

Most samples show wide, variable t-T paths for early Miocene but have narrow, well constrained t-T paths for middle-late Miocene cooling (Fig. 9). Modeling results are based on at least 100 good fits (Table 3). We interpret the good fit paths to represent cooling through the HePRZ and apatite (A)PAZ due to exhumation. In general, our inverse models reflect northeastward younging along the Tila River.

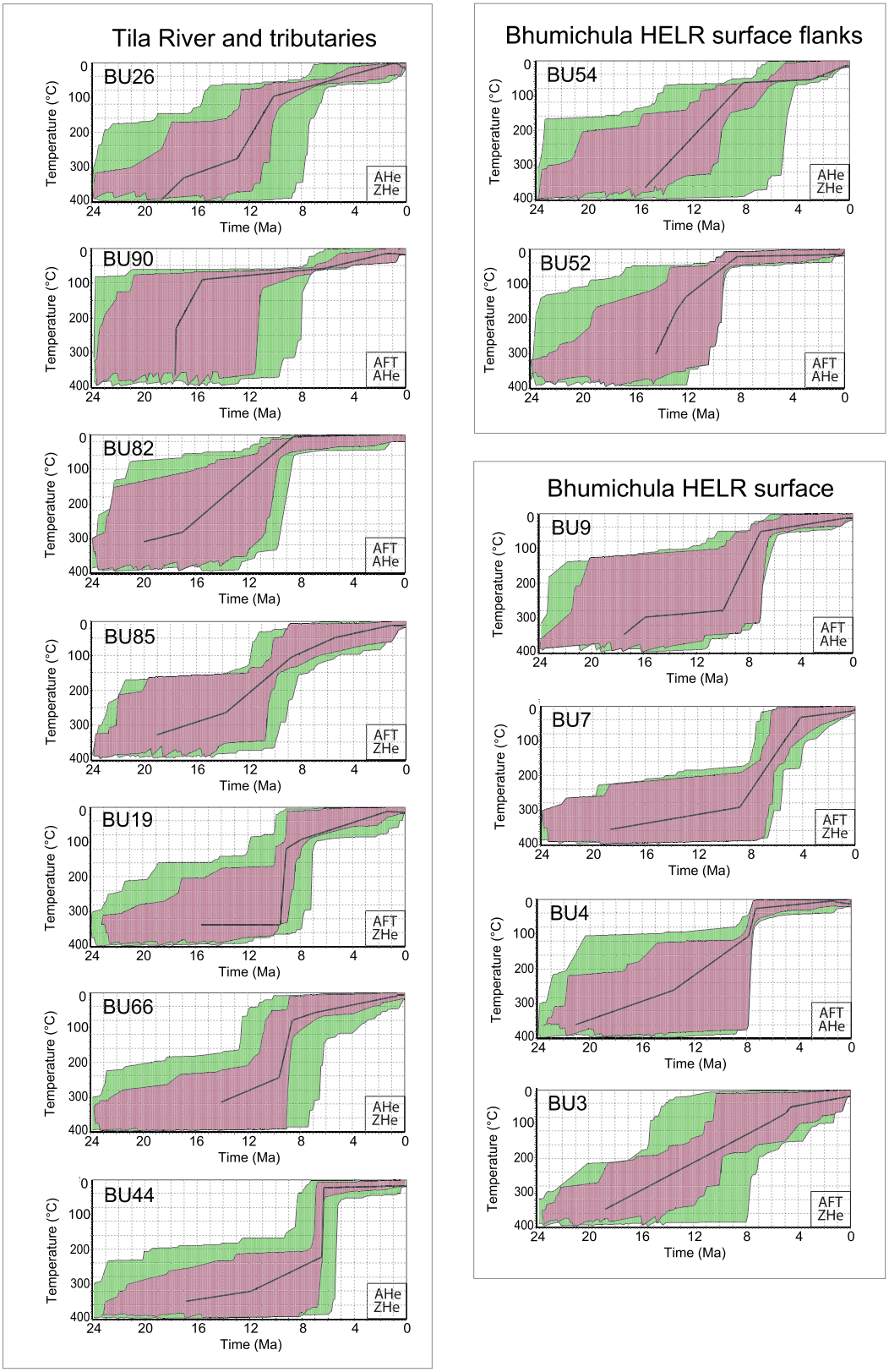

Figure 9. Thermal history models generated by inverse modeling in HeFTy v1.9.3 for samples from the northeast limb of Dadeldhura synform. Time-temperature paths show inverse models based on a combination of zircon (U-Th-Sm)/He (ZHe), apatite fission track (AFT), and apatite (U-Th-Sm)/He (AHe) data. Samples BU3, BU4, BU7, and BU9 are from the Bhumichula plateau; BU54 and BU52 are from a ridge descending down the southwestern flank of the plateau. Samples BU90, BU82, BU85, BU19, BU66, and BU44 are samples along the Tila River and its tributaries whereas BU26 is a sample at the confluence of the Karnali and Tila rivers. Green envelopes indicate acceptable paths (with goodness of fit >0.5) and purple envelopes indicate good paths (with goodness of fit >0.05). All models start at an initial T-window between 400 °C and 300 °C at ca. 24–14 Ma based on published ^{40}Ar-^{39}Ar white mica ages and geological constraints, and end between 20 °C and 0 °C at ca. 2–0 Ma. Additional information is provided in the text and Table 3. The partial retention zone temperature range is ~40–70 °C for the AHe system and ~165–195 °C for the ZHe system. The partial annealing zone temperature range for the AFT system is ~120–80 °C. HELR—high-elevation low-relief.

BU26, BU90, BU85, and BU82 all exhume through the HePRZ and APAZ at >10 Ma, whereas BU19 and BU66 cool through the HePRZ and APAZ ca. 10–6 Ma (Fig. 9). The easternmost sample, BU44, cools between ca. 7 and ca. 6 Ma.

Similarly, samples on the Bhumichula plateau show a subtle younging with increasing elevation. BU54 and BU52, collected from

the southern flank of the plateau, show cooling through the HePRZ and APAZ between ca. 14 Ma and ca. 8 Ma but a wide range of older cooling paths is also observed (Fig. 9). Bhumichula surface samples also have a wide range of possible cooling paths prior to the early Miocene so we focus on the middle-late Miocene cooling. Samples BU9, BU7, BU4, and BU3 show gradual cooling through zircon HePRZ and APAZ between ca. 12 Ma and ca. 7 Ma and apatite HePRZ between ca. 10 Ma and ca. 5 Ma (Fig. 9).

The AHe and ZHe ages show inter-sample and intra-sample age dispersion which is a function of protracted residence in the PRZ and eU. We therefore emphasize our AFT data and thermal history models, which account for radiation damage accumulation and protracted residence in the PRZ, to reflect cooling history of our samples. All thermochronometer data sets not modeled are independently and mutually consistent with thermal history models validating our assumptions.

SUMMARY AND DISCUSSION

We use AFT, AHe, and ZHe cooling ages along with inverse thermal history models using HeFTy to investigate the exhumation history of the Bhumichula plateau. Hypothesis 1 suggests that the Bhumichula plateau is a low relief landscape that formed at low elevations and was later uplifted to higher elevations, whereas Hypothesis 2 suggests that the plateau is a remnant of an extensive paleolandscape that formed as it rose to high elevations and was simultaneously incised by an antecedent river (Fig. 6). Hypothesis 3 is similar to Hypothesis 2 but in this scenario, rivers incise the elevated region by knickpoint migration and/or headward erosion (Fig. 6).

Hypothesis (1) can be readily discarded because it is incompatible with basic geological information: The Bhumichula HELR surface cuts across the folded northern limb of the synformal Dadeldhura klippe, which requires that the surface post-dates significant crustal thickening and folding above the south limb of the Lesser Himalayan duplex (Figs. 2 and 5). Several hundred kilometers of tectonic shortening during emplacement of the Main Central and Ramgarh thrust sheets and growth of the Lesser Himalayan duplex caused significant crustal thickening (Fig. 5; Robinson et al., 2006; DeCelles et al., 2020). Isostatic rise of high topography must have accompanied this crustal thickening, as demonstrated by the synorogenic sedimentary record of the Himalayan foreland basin (e.g., Tokuoka et al., 1986; Critelli and Garzanti, 1994; Burbank et al., 1996; Uddin and Lundberg, 1998; DeCelles et al., 1998, 2004, 2014; Raiverman et al., 1983; Najman and Garzanti, 2000; Najman, 2006; Szulc et al., 2006; Ravikant et al., 2011; Garzanti, 2019; and many others). Therefore, the Bhumichula HELR surface must have formed after significant elevation had already been attained by the rocks upon which it formed.

Having rejected Hypothesis (1) on the basis of geological relationships, we revisit Hypotheses (2) and (3), which are readily testable with our thermochronologic data. Hypothesis (2) predicts increasing low-temperature cooling ages upstream at higher elevations, especially on the Bhumichula HELR surface following a classic age versus elevation cooling trend, whereas Hypothesis (3) predicts ages that decrease both upstream and at progressively higher elevations. ZHe, AFT, and AHe ages are between ca. 10 Ma and ca. 5 Ma on the Bhumichula plateau and ca. 14 Ma and ca. 6 Ma along the Tila River. Both ZHe and AFT data reflect upstream younging along the Tila River and its tributaries, which suggests that incision advanced northeastward along the Tila River and southward toward the Bhumichula plateau from ca.14 Ma until ca. 6 Ma (Fig. 8). Our age-elevation data show an inverse relationship in which cooling ages decrease with increasing elevation (Fig. 8; Ehlers and Farley, 2003), but we recognized that the samples do not follow a perfect age-elevation trend and are too far apart for a true "vertical profile." Nevertheless, this inverse age-elevation relationship may be significant and likely is a function of upstream propagation of incision either by headward erosion or knickpoint migration. Although our data cannot distinguish between headward erosion, divide migration, and knickpoint migration, they do suggest an overall laterally migrating wave of erosion toward what remains of the HELR surface. Our age-elevation data suggest Hypothesis (2) is unlikely because progressive erosion of rocks moving upward through their cooling isotherms would result in relatively older ages at higher elevations.

Based on structural relationships, the Bhumichula HELR surface is a post-kinematic surface that was beveled after Greater Himalayan Sequence rocks were tipped upward by growth of the underlying Lesser Himalayan duplex. Our cooling ages constrain the timing of the last major exhumation and rock uplift to the late Miocene (ca. 7–5 Ma). The Bhumichula HELR surface was most likely at high elevations at this time because of extreme crustal shortening and thickening, and experienced reduction in relief due to mechanisms such as glaciation or drainage reorganization. We therefore suggest that the Bhumichula plateau is a remnant of a more extensive high-elevation paleolandscape that has been isolated due to upstream propagation of incision along tributaries of the Karnali and Tila rivers and subsequently experienced localized relief reduction by glacial beveling (Figs. 10 and 11).

Previous studies have shown that during the early Miocene, the Main Central thrust placed GHS rocks on top of LHS rocks regionally (Figs. 2 and 5; e.g., DeCelles et al., 2001; Robinson et al., 2006; Soucy La Roche et al., 2018a, 2018b), whereas during the middle to late Miocene, the Ramgarh thrust emplaced older LHS rocks on top of younger LHS rocks (e.g., Robinson et al., 2006). The Ramgarh thrust also served as the roof thrust for the Lesser Himalayan duplex (e.g., Srivastava and Mitra, 1994; DeCelles et al., 2001, 2020; Pearson and DeCelles, 2005; Robinson et al., 2006; Mitra et al., 2010; Robinson and Martin, 2014), a large antiformal duplex that caused arching of the overlying Lesser, Greater, and Tethyan Himalayan rocks during late Miocene time (Figs. 11B and 11C). Published low-temperature thermochronology from the Dadeldhura klippe indicates AFT ages between ca. 9 and ca. 6 Ma (van der Beek et al., 2016) along the Karnali River (Fig. 7), and ZHe ages between ca. 14 and ca. 10 Ma and AFT ages between ca. 10 and ca. 4 Ma (DeCelles et al., 2020) in the western Dadeldhura klippe. New ZHe, AFT, and AHe data reported in this study (Table 1) support the interpretation that significant exhumation of the Dadeldhura klippe rocks occurred during the early Miocene due to MCT emplacement and during the middle-late Miocene due to Ramgarh thrust displacement, growth of the Lesser Himalayan duplex, and passive uplift of the overlying MCT sheet (Figs. 5 and 11).

Although low temperature thermochronology does not directly constrain surface uplift, we infer that the last major period of exhumation and uplift along the Tila River and the Bhumichula plateau occurred between ca. 14 Ma (at least) and ca. 5 Ma, and that the plateau has since experienced low rates of exhumation. We assume a geothermal gradient of 25 °C/km and use our ZHe, AFT, and AHe cooling dates to calculate exhumation rates focusing on cooling through closure temperatures of our thermochronometers. Studies in the western (Bhattacharya et al., 2020) or eastern Himalaya (Carrapa et al., 2016) use a range of 20–30 °C/km. Exhumation rates vary between ca. 0.3 and ca. 1.3 mm/yr for samples along the Tila River (BU26, BU90, BU89, BU82, BU85, BU19, BU70, BU66, BU44), between ca. 0.3 and ca.0.7 mm/yr on the flanks of the Bhumichula plateau (BU51, BU54, BU52), and between ca. 0.4 and ca.1 mm/yr for the Bhumichula plateau samples. Exhumation rates average to ~0.6 mm/yr along the Tila River, ~0.4 mm/yr on the Bhumichula flanks, and ~0.5 mm/yr on the surface

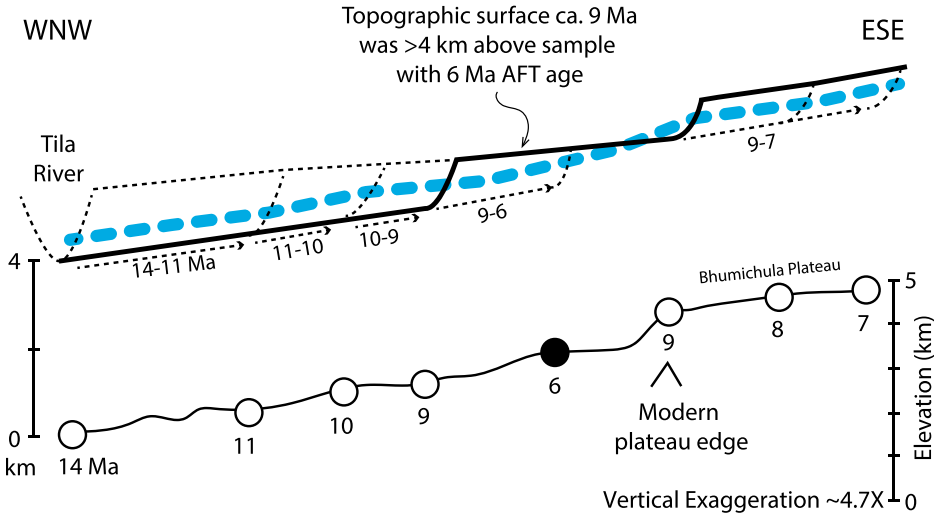

Figure 10. Schematic stream-wise erosional profile on northwest flank of the Bhumichula plateau designed to explain the age versus elevation trends of zircon (U-Th-Sm)/He and apatite fission track (AFT) ages shown in Figure 8. Lower profile is schematic present topography with average AFT cooling ages indicated by numbered open circles. Bold blue dashed line represents an imaginary surface projected a vertical distance of 4 km above the lower profile (i.e., the minimum overburden required to account for the cooling ages, assuming a geothermal gradient of 25 °C/km). Bold black line shows topographic surface at ca. 9 Ma. Dashed thin black lines and arrows in upper profile show the east-southeastward retreat of topography as a major knickpoint in the Tila River system migrated headward, with times based on ranges of AFT ages. If the topographic surface (indicated by black dashed and solid lines in upper profile) at any point along the upper profile was below the blue dashed line at any time, the rocks on the lower profile would register a cooling age at that time. If the topographic surface was above the blue dashed line at any point, the rocks below that point would have remained hotter than the AFT closure temperature. Note that two separate locations along the lower profile, separated by ~1600 m vertical distance, must have cooled through the top of the AFT closure temperature by ca. 9 Ma, whereas the intervening area remained relatively hot until ca. 6 Ma. Bold solid line in the upper profile shows a schematic surface topography at ca. 9 Ma that could have resulted in the age versus elevation pattern. Bold circle highlights the plateau edge at ca. 9 Ma.

of the Bhumichula HELR surface. It is important to note that these exhumation rates are minimum average estimates based on the closure temperature of our highest temperature thermochronometer, ZHe (~180 °C), and assuming steady-state conditions. Slow exhumation rates on the Bhumichula plateau since the late Miocene are consistent with our interpretation that the Bhumichula HELR is a paleolandscape that has not yet been incised. Slow erosion and incision can be linked to glacially induced relief reduction and/or increased snowfall at the expense of rain leading to a reduction in threshold-exceeding floods.

Additionally, we calculated minimum estimates of exhumation and incision upstream along the Tila River. Our lowest sample at the confluence of the Tila and Karnali rivers (BU26) has cooling ages between ca. 11 Ma and ca. 7 Ma whereas the highest sample upstream along the Tila River (BU66) has cooling ages of ca. 6 Ma, which indicates that incision migrated ~53 km upstream over a timespan of 1–5 million years. The resulting average upstream incision rates of ~10–53 mm/yr are comparable to knickpoint migration rates of 4 mm/yr to 10^6 mm/yr calculated over shorter timescales for a range of drainage areas (Loget and Driessche, 2009; Mackey et al., 2014).

In detail, ZHe and AFT age versus elevation profiles (Fig. 8) suggest that the paleotopographic surface of the Bhumichula plateau had a stepped profile at ca. 9 Ma and possibly before and after that time (Fig. 10). This is required to explain the abrupt increase in cooling ages at the present edge of the plateau on its northern side (Fig. 8). Figure 10 depicts a relationship between paleotopography and AFT cooling ages that is capable of explaining the age distribution, assuming rapid cooling through the 120 °C isotherm and a geothermal gradient of 25 °C/km.

Paleoaltimetry studies based on hydrogen isotope ratios (δD) in the Mt. Everest region of eastern Nepal report near-modern elevations of 5100–5400 m during the early Miocene (Gébelin et al., 2013). Low-temperature cooling ages from the north flank of Mt. Everest are predominantly early to middle Miocene (Carrapa et al., 2016; Orme et al., 2015), whereas ages reported from the south flank of the mountain are <5 Ma (Streule et al., 2012). Carrapa et al. (2016) suggested that this pattern, coupled with the high paleoelevation reconstructed by Gébelin et al. (2013), reflects upstream incision into a high elevation region in the hanging wall of the MCT. A similar landscape evolution in western Nepal would suggest that a high elevation region might have been present in the area occupied by the Dadeldhura klippe by middle to late Miocene time, in agreement with our data (Fig. 7). The Karnali River may or may not have been flowing through this area at that time, but our cooling ages suggest that as the Ramgarh thrust sheet became active and the Lesser Himalayan duplex grew and folded overlying rocks of the Dadeldhura (Main Central) thrust sheet, rivers in this region responded by increased incision, thereby carving into the paleosurface (Fig. 11).

Drainage reorganization has been proposed as a mechanism for low relief formation at high elevations (Yang et al., 2015) where a tectonic forcing causes rapidly incising streams from an expanding basin to gain drainage area at the expense of a neighboring shrinking basin. This "area-loss feedback" model (Willett et al., 2014) involves a positive feedback loop in which drainage area loss further diminishes erosion and induces local aggradation. An asymmetric coincident divide develops along the boundary between the expanding and shrinking drainage basins. We observe similar coincident divides on the southeastern and northeastern parts of the Bhumichula plateau (Fig. 3B), which implies that drainage area loss may have helped to reduce relief on the Bhumichula plateau.

Glaciation also probably influenced low relief formation on the Bhumichula plateau. Northern hemisphere glaciation developed during the late Pliocene-early Pleistocene (Hayashi et al., 2020) and several studies have suggested extensive glaciation in the Himalaya during Pleistocene-Holocene time (Brozović et al., 1997; Owen, 2009). The presence of multiple glacial lakes and moraines on the Bhumichula plateau indicates past glaciation. However, if Bhumichula plateau had been exhumed and uplifted near the modern equilibrium-line altitude (ELA) during the late Miocene, it could have experienced alpine glaciation and relief reduction since then. Contemporary steady-state ELAs vary between 4500 and 6000 m asl in the northwestern Himalaya (Saha et al., 2019a, 2019b), which is within the elevation range of the Bhumichula plateau. Although the ELA has fluctuated since late Miocene, the prevalence of the Bhumichula

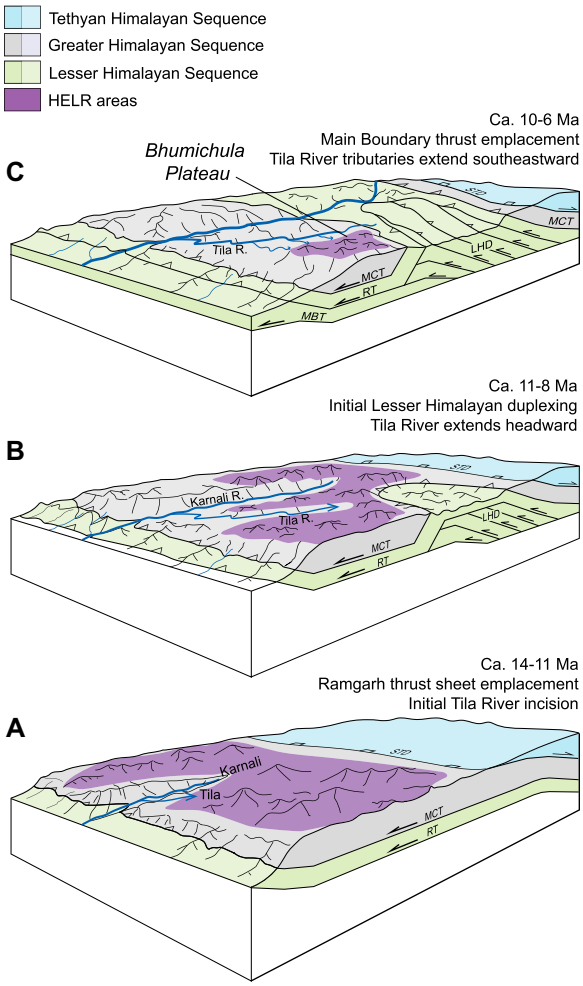

Figure 11. Three-dimensional block diagrams illustrating proposed development of the Bhumichula plateau within the kinematic context of the Main Central (MCT), Ramgarh (RT), and Main Boundary (MBT) thrusting and growth of the Lesser Himalayan duplex (LHD). Northward and eastward extension of the Karnali and Tila rivers, respectively, is shown schematically. Arrowheads indicate directions of headward erosion, not flow directions. Not depicted is the period of Pleistocene glaciation that would have strongly beveled topography on the plateau to produce the present low-relief. STD represents the South Tibetan detachment system, which is omitted from the Dadeldhura klippe (Soucy La Roche et al., 2018a) for clarity. HELR—high-elevation low-relief.

plateau's peak elevations near modern ELAs suggest that glaciers eroded headward but not deeply, and may have limited maximum elevations (e.g., Brozović et al., 1997; Egholm et al., 2009; Zhang et al., 2016). Furthermore, glaciation might further flatten the topography if the initial landscape has low relief (Pedersen et al., 2014); the Bhumichula area might have had relatively low relief prior to glaciation because of lithological uniformity and structural simplicity over much of the Dadeldhura klippe. Himalayan glaciation is controlled by the winter midlatitude westerlies (Owen et al., 1998; Benn and Owen, 1998) and summer South Asian Monsoon, which were well established by ca. 11 Ma (Dettman et al., 2001) and possibly earlier (Clift and Webb, 2019). Thus, by late Miocene, near-modern monsoonal precipitation and elevations near ELA could have facilitated growth of temperate alpine glaciers on the Bhumichula plateau. Glacial erosion may have helped to produce low relief on the Bhumichula plateau but it is unlikely to have exhumed rocks through ZHe, AFT, and AHe closure temperatures. We suggest that the Bhumichula HELR landscape was produced by surface uplift to elevations sufficient to maintain alpine glaciers, which eroded laterally to produce low relief above the ELA.

Upstream incision by major rivers either by knickpoint migration or headward erosion isolated the shrinking Bhumichula plateau as a remnant of a once more widespread high-elevation landscape (Fig. 11). Given the fact that permanent snow and ice are not present on the Bhumichula plateau today, we suggest that the plateau resides within a narrow range of elevation (~4200–4800 m) that is too low for active glaciation but too high for large amounts of rainfall; most precipitation falls as sleet and snow, and winter snow is typically melted off by early summer. This, together with small drainage basin size and low slopes, may minimize fluvial erosion, helping to preserve what remains of the plateau.

Given the widespread occurrence of HELR surfaces in the Himalaya (Grujic et al., 2006; Adams et al., 2015, 2016) and their association with Greater Himalayan Sequence substrates (e.g., Grujic et al., 2006), it seems likely that, in general, these surfaces might represent remnants of a once far more extensive HELR landscape that extended southward nearly to the front of the Himalaya. Greater Himalayan rocks in eastern Nepal reach to within as little as 15 km of the range front, and are increasingly widespread in Sikkim, Bhutan, and Arunachal Pradesh except where breached by erosional/structural windows. Increased preservation of Greater Himalayan rocks in the eastern Himalaya is partly related to less structural relief in the Lesser Himalayan duplex (e.g., Long and Robinson, 2021), but also must be related to greater rates of erosion in the central sector of the orogen (Thiede and Ehlers, 2013; DeCelles and Carrapa, 2021). This is also reflected by generally higher, range-transverse convex topography in the eastern Himalaya and lower elevation, range-transverse concave topography in the central Himalaya, with the transition occurring in eastern Nepal (Yin, 2006). In eastern Nepal, post-Miocene headward erosion by southward flowing fluvial drainages in the Okhaldhunga structural window has pushed the zone of high elevation northward (Carrapa et al., 2016) whereas in Bhutan, Greater Himalayan rocks extend far to the south (Grujic et al., 2006). We suggest that relatively high elevation tracks the distribution of Greater Himalayan high-grade metamorphic rocks because of their durability (Cannon et al., 2018) relative to less erosionally resistant phyllites that dominate the structurally underlying Lesser Himalayan Sequence. Where elevation reached the ELA of 4000–4500 m by tectonic processes, glacial buzzsaw processes efficiently leveled topography by lateral headward erosion at glacier headwalls (e.g., Egholm et al., 2009; Dortch et al., 2011; Buceta et al., 2020). Both drainage area loss and glaciation could have promoted lower relief on the plateau surface.

If HELR surfaces in the Himalaya are indeed remnants of a more widespread high elevation landscape, then the erosion of landscapes surrounding relict HELR surfaces represents a sizeable degradation of the mass and bulk of the Himalayan orogenic wedge since the time of the development of the HELR surfaces. Future studies linking HELR surfaces along the southern slope of the Himalaya might provide temporally constrained estimates of mass efflux from the range.

CONCLUSIONS

Although thermochronologic data do not directly constrain surface uplift and paleoelevation, when combined with other geological and geomorphological evidence, our multidisciplinary dataset in western Nepal suggest that periods of exhumation coincide with periods of rock uplift associated with thrust activity and duplex development. Rapid exhumation during

the middle-late Miocene is coincident with the timing of regionally prevalent emplacement of the Ramgarh thrust sheet and growth of the Lesser Himalayan duplex. Significant crustal thickening since early Miocene time must have driven rock and surface uplift, and progressive upstream incision since then has removed high topography with the exception of the Bhumichula plateau. The last major pulse of exhumation on the Bhumichula plateau and along the Tila River initiated during the middle Miocene, suggesting the plateau surface had been uplifted to relatively high elevations (~4–5 km) by then. Younger cooling ages reflect progressive fluvial incision into the paleolandscape, which has isolated the Bhumichula plateau. Since the late Miocene, the Bhumichula plateau has developed and preserved low-relief either due to a lag in fluvial incision, drainage reorganization and in situ relief reduction, or a combination of the two in conjunction with alpine glaciation. Consideration of the distribution of high elevation/low relief landscapes in the Himalaya suggests that erosion since late Miocene time has been more rapid in the central Himalaya than in the eastern Himalaya.

ACKNOWLEDGMENTS

The authors would like to acknowledge Willy Guenthner, Sean Long, and an anonymous reviewer for constructive reviews. We thank Jay Quade for productive feedback during initial drafts of this manuscript. We also thank the Arizona Radiogenic Helium Dating Laboratory (Tucson, USA) for assistance in acquiring (U-Th-Sm)/He data and Gilby Jepson for assistance with preparing samples for apatite fission track analysis. Dr. T.P. Ojha, Dr. Ananta Gajurel, and C. Pokharel helped with permitting, logistical issues, and sample shipping. Field research permits were provided by the Nepal Department of Mines and Geology. We gratefully acknowledge Bhairab Sitaula, Bhai Kaji Tamang, Tall Bahadur Tamang, and all the Nepalese field support staff who helped with sample collection and made this project possible. This research was supported by grants from the National Science Foundation (EAR 1763432) and the National Geographic Society.

REFERENCES CITED

Abbott, L.D., Silver, E.A., Anderson, R.S., Smith, R., Ingle, J.C., Kling, S.A., Haig, D., Small, E., Galewsky, J., and Sliter, W., 1997, Measurement of tectonic surface uplift rate in a young collisional mountain belt: Nature, v. 385, p. 501–507, https://doi.org/10.1038/385501a0.

Adams, B.A., Hodges, K.V., Whipple, K.X., Ehlers, T.A., Van Soest, M.C., and Wartho, J., 2015, Constraints on the tectonic and landscape evolution of the Bhutan Himalaya from thermochronometry: Tectonics, v. 34, p. 1329–1347, https://doi.org/10.1002/2015TC003853.

Adams, B.A., Whipple, K.X., Hodges, K.V., and Heimsath, A.M., 2016, In situ development of high-elevation, low-relief landscapes via duplex deformation in the Eastern Himalayan hinterland, Bhutan: Journal of Geophysical Research. Earth Surface, v. 121, p. 294–319, https://doi.org/10.1002/2015JF003508.

Andermann, C., Longuevergne, L., Bonnet, S., Crave, A., Davy, P., and Gloaguen, R., 2012, Impact of transient groundwater storage on the discharge of Himalayan rivers: Nature Geoscience, v. 5, p. 127–132, https://doi.org/10.1038/ngeo1356.

Ault, A.K., Gautheron, C., and King, G.E., 2019, Innovations in (U-Th)/He, fission track, and trapped charge thermochronometry with applications to earthquakes, weathering, surface-mantle connections, and the growth and decay of mountains: Tectonics, v. 38, p. 3705–3739, https://doi.org/10.1029/2018TC005312.

Barbarand, J., Carter, A., Wood, I., and Hurford, T., 2003, Compositional and structural control of fission-track annealing in apatite: Chemical Geology, v. 198, p. 107–137, https://doi.org/10.1016/S0009-2541(02)00424-2.

Benn, D.I., and Owen, L.A., 1998, The role of the Indian summer monsoon and the mid-latitude westerlies in Himalayan glaciation: Review and speculative discussion: Journal of the Geological Society, v. 155, p. 353–363, https://doi.org/10.1144/gsjgs.155.2.0353.

Bhattacharya, G., Robinson, D.M., Orme, D.A., Najman, Y., and Carter, A., 2020, Low-temperature thermochronology of the Indus Basin in central Ladakh, northwest India: Implications of Miocene-Pliocene cooling in the India-Asia collision zone: Tectonics, v. 39, https://doi.org/10.1029/2020TC006333.

Blythe, A.E., Burbank, D.W., Carter, A., Schmidt, K., and Putkonen, J., 2007, Plio-Quaternary exhumation history of the central Nepalese Himalaya: 1. Apatite and zircon fission track and apatite [U-Th]/He analyses: Tectonics, v. 26, no. 3, https://doi.org/10.1029/2006TC001990.

Bohlinger, P., and Sorteberg, A., 2017, A comprehensive view on trends in extreme precipitation in Nepal and their spatial distribution: International Journal of Climatology, v. 38, p. 1833–1845, https://doi.org/10.1002/joc.5299.

Bookhagen, B., and Burbank, D.W., 2010, Toward a complete Himalayan hydrological budget: Spatiotemporal distribution of snowmelt and rainfall and their impact on river discharge: Journal of Geophysical Research. Earth Surface, v. 115, https://doi.org/10.1029/2009JF001426.

Braden, Z., Godin, L., and Cottle, J.M., 2017, Segmentation and rejuvenation of the Greater Himalayan sequence in western Nepal revealed by in situ U-Th/Pb monazite petrochronology: Lithos, v. 284–285, p. 751–765, https://doi.org/10.1016/j.lithos.2017.04.023.

Braden, Z., Godin, L., Cottle, J., and Yakymchuk, C., 2018, Renewed late Miocene (<8 Ma) hinterland ductile thrusting, western Nepal Himalaya: Geology, v. 46, p. 503–506, https://doi.org/10.1130/G40097.1.

Brozović, N., Burbank, D.W., and Meigs, A.J., 1997, Climatic limits on landscape development in the northwestern Himalaya: Science, v. 276, p. 571–574, https://doi.org/10.1126/science.276.5312.571.

Buceta, R.E., Schoenbohm, L.M., and DeCelles, P.G., 2020, Glacial and fluvial erosion in the Dolpo Basin, Western Nepal: Geomorphology, v. 354, https://doi.org/10.1016/j.geomorph.2020.107033.

Burbank, D.W., Leland, J., Fielding, E., Anderson, R.S., Brozovic, N., Reid, M.R., and Duncan, C., 1996, Bedrock incision, rock uplift and threshold hillslopes in the northwestern Himalayas: Nature, v. 379, p. 505–510, https://doi.org/10.1038/379505a0.

Burbank, D.W., Bookhagen, B., Gabet, E.J., and Purkonen, J., 2012, Modern climate and erosion in the Himalaya: Comptes Rendus Geoscience, v. 344, p. 610–626, https://doi.org/10.1016/j.crte.2012.10.010.

Calvet, M., Gunnell, Y., and Farines, B., 2015, Flat-topped mountain ranges: Their global distribution and value for understanding the evolution of mountain topography: Geomorphology, v. 241, p. 255–291, https://doi.org/10.1016/j.geomorph.2015.04.015.

Cannon, J.M., Murphy, M.A., and Taylor, M., 2018, Segmented strain accumulation in the High Himalaya expressed in river channel steepness: Geosphere, v. 14, p. 1131–1149, https://doi.org/10.1130/GES01508.1.

Carosi, R., Musumeci, G., and Pertusati, P.C., 1999, Extensional tectonics in the higher Himalayan crystallines of Khumbu Himal, eastern Nepal, *in* Macfarlane, A., Sorkhabi, R.B., and Quade, J., Himalaya and Tibet: Mountain Roots to Mountain Tops: Geological Society of America Special Paper, v. 328, p. 211–223, https://doi.org/10.1130/0-8137-2328-0.211.

Carrapa, B., Robert, X., DeCelles, P.G., Orme, D.A., Thomson, S.N., and Schoenbohm, L.M., 2016, Asymmetric exhumation of the Mount Everest region: Implications for the tectono-topographic evolution of the Himalaya: Geology, v. 44, p. 611–614, https://doi.org/10.1130/G37756.1.

Carrapa, B., DeCelles, P.G., and Romero, M., 2019, Early Inception of the Laramide Orogeny in Southwestern Montana and Northern Wyoming: Implications for Models of Flat-Slab Subduction: Journal of Geophysical Research. Solid Earth, v. 124, p. 2102–2123, https://doi.org/10.1029/2018JB016888.

Clark, M.K., House, M.A., Royden, L.H., Whipple, K.X., Burchfiel, B.C., Zhang, X., and Tang, W., 2005, Late Cenozoic uplift of southeastern Tibet: Geology, v. 33, p. 525–528, https://doi.org/10.1130/G21265.1.

Clark, M.K., Royden, L.H., Whipple, K.X., Burchfiel, B.C., Zhang, X., and Tang, W., 2006, Use of a regional, relict landscape to measure vertical deformation of the eastern Tibetan Plateau: Journal of Geophysical Research. Earth Surface, v. 111, F3, https://doi.org/10.1029/2005JF000294.

Clift, P.D., and Webb, A.A.G., 2019, A history of the Asian monsoon and its interactions with solid Earth tectonics in Cenozoic South Asia, *in* Treloar, P.J., and Searle, M.P., eds., Himalayan Tectonics: A Modern Synthesis: Geological Society of London Special Publications, v. 483, p. 631–652, https://doi.org/10.1144/SP483.1.

Copeland, P., 2015, $^{40}Ar/^{39}Ar$ ages of muscovites from modern Himalayan rivers: Himalayan evolution and the relative contribution of tectonics and climate, Geosphere v. 11, p. 1837–1859, https://doi.org/10.1130/GES01154.1.

Critelli, S., and Garzanti, E., 1994, Provenance of the Lower Tertiary Murree redbeds (Hazara-Kashmir Syntaxis, Pakistan) and initial rising of the Himalayas: Sedimentary Geology, v. 89, p. 265–284, https://doi.org/10.1016/0037-0738(94)90097-3.

Curray, J.R., Emmel, F.J., and Moore, D.G., 2002, The Bengal Fan: Morphology, geometry, stratigraphy, history and processes: Marine and Petroleum Geology, v. 19, p. 1191–1223, https://doi.org/10.1016/S0264-8172(03)00035-7.

DeCelles, P.G., and Carrapa, B., 2021, Coupled rapid erosion and foreland sedimentation control orogenic wedge kinematics in the Himalayan Thrust Belt of central Nepal: Journal of Geophysical Research. Solid Earth, v. 126, https://doi.org/10.1029/2020JB021256.

DeCelles, P.G., Gehrels, G.E., Quade, J., and Ojha, T.P., 1998, Eocene-early Miocene foreland basin development and the history of Himalayan thrusting, western and central Nepal: Tectonics, v. 17, p. 741–765, https://doi.org/10.1029/98TC02598.

DeCelles, P.G., Robinson, D.M., Quade, J., Ojha, T.P., Garzione, C.N., Copeland, P., and Upreti, B.N., 2001, Stratigraphy, structure, and tectonic evolution of the Himalayan fold-thrust belt in Western Nepal: Tectonics, v. 20, p. 487–509, https://doi.org/10.1029/2000TC001226.

DeCelles, P.G., Gehrels, G.E., Najman, Y., Martin, A.J., Carter, A., and Garzanti, E., 2004, Detrital geochronology and geochemistry of Cretaceous–Early Miocene strata of Nepal: Implications for timing and diachroneity of initial Himalayan orogenesis: Earth and Planetary Science Letters, v. 227, p. 313–330, https://doi.org/10.1016/j.epsl.2004.08.019.

DeCelles, P.G., Kapp, P., Gehrels, G.E., and Ding, L., 2014, Paleocene-Eocene foreland basin evolution in the Himalaya of southern Tibet and Nepal: Implications for the age of initial India-Asia collision: Tectonics, v. 33, p. 824–849, https://doi.org/10.1002/2014TC003522.

DeCelles, P.G., Carrapa, B., Ojha, T.P., Gehrels, G.E., and Collins, D., 2020, Structural and thermal evolution of the Himalayan Thrust Belt in midwestern Nepal: Geological Society of America Special Papers, v. 547, 79 p., https://doi.org/10.1130/2020.2547(01).

Dettman, D.L., Kohn, M.J., Quade, J., Ryerson, F.J., Ojha, T.P., and Hamidullah, S., 2001, Seasonal stable isotope evidence for a strong Asian monsoon throughout the past 10.7 m.y.: Geology, v. 29, p. 31–34, https://doi.org/10.1130/0091-7613(2001)029<0031:SSIEFA>2.0.CO;2.

Ding, L., Qasim, M., Jadoon, I.A.K., Khan, M.A., Xu, Q., Cai, F., Wang, H., Baral, U., and Yue, Y., 2016, The India-Asia collision in north Pakistan: Insight from the

U-Pb detrital zircon provenance of Cenozoic foreland basin: Earth and Planetary Science Letters, v. 455, p. 49–61, https://doi.org/10.1016/j.epsl.2016.09.003.

Donelick, R.A., Ketcham, R.A., and Carlson, W.D., 1999, Variability of apatite fission-track annealing kinetics: II. Crystallographic orientation effects: The American Mineralogist, v. 84, p. 1224–1234, https://doi.org/10.2138/am-1999-0902.

Donelick, R.A., O'Sullivan, P.B., and Ketcham, R.A., 2005, Apatite fission-track analysis: Reviews in Mineralogy and Geochemistry, v. 58, p. 49–94, https://doi.org/10.2138/rmg.2005.58.3.

Dortch, J.M., Owen, L.A., Schoenbohm, L.M., and Caffee, M.W., 2011, Asymmetrical erosion and morphological development of the central Ladakh Range, northern India: Geomorphology, v. 135, p. 167–180, https://doi.org/10.1016/j.geomorph.2011.08.014.

Duncan, C., Masek, J., and Fielding, E., 2003, How steep are the Himalaya? Characteristics and implications of along-strike topographic variations: Geology, v. 31, p. 75–78, https://doi.org/10.1130/0091-7613(2003)031<0075:HSATHC>2.0.CO;2.

Egholm, D.L., Nielsen, S.B., Pedersen, V.K., and Lesemann, J.E., 2009, Glacial effects limiting mountain height: Nature, v. 460, p. 884–887, https://doi.org/10.1038/nature08263.

Ehlers, T.A., and Farley, K.A., 2003, Apatite (U-Th)/He thermochronometry: Methods and applications to problems in tectonic and surface processes: Earth and Planetary Science Letters, v. 206, p. 1–14, https://doi.org/10.1016/S0012-821X(02)01069-5.

Epis, R., and Chapin, C., 1975, Geomorphic and tectonic implications of the post-Laramide, late Eocene erosion surface in the southern Rocky Mountains, in Curtis, B.F., ed., Cenozoic history of the Southern Rocky Mountains: Geological Society of America Memoir, v. 144, p. 45–74.

Farley, K.A., 2002, (U-Th)/He dating: Techniques, calibrations, and applications: Reviews in Mineralogy and Geochemistry, v. 47, p. 819–844, https://doi.org/10.2138/rmg.2002.47.18.

Farley, K.A., Shuster, D.L., and Ketcham, R.A., 2011, U and Th zonation in apatite observed by laser ablation ICPMS, and implications for the (U-Th)/He system: Geochimica et Cosmochimica Acta, v. 75, p. 4515–4530, https://doi.org/10.1016/j.gca.2011.05.020.

Fielding, E., Isacks, B., Barazangi, M., and Duncan, C., 1994, How flat is Tibet?: Geology, v. 22, p. 163–167, https://doi.org/10.1130/0091-7613(1994)022<0163:HFIT>2.3.CO;2.

Fitzgerald, P.G., and Stump, E., 1995, Uplift and denudation of the central Alaska Range: A case study in the use of apatite fission track thermochronology to determine absolute uplift parameters: Journal of Geophysical Research. Solid Earth, v. 100, p. 20,175–20,919, https://doi.org/10.1029/95JB02150.

Fitzgerald, P.G., Baldwin, S.L., Webb, L.E., and O'Sullivan, P.B., 2006, Interpretation of (U-Th)/He single grain ages from slowly cooled crustal terranes: A case study from the Transantarctic Mountains of southern Victoria Land: Chemical Geology, v. 225, p. 91–120, https://doi.org/10.1029/95JB02150.

Flint, J.J., 1974, Stream gradient as a function of order, magnitude, and discharge: Water Resources Research, v. 10, p. 969–973, https://doi.org/10.1029/WR010i005p00969.

Flowers, R.M., Shuster, D.L., Wernicke, B.P., and Farley, K.A., 2007, Radiation damage control on apatite (U-Th)/He dates from the Grand Canyon region, Colorado Plateau: Geology, v. 35, p. 447–450, https://doi.org/10.1130/G23471A.1.

Flowers, R.M., Ketcham, R.A., Shuster, D.L., and Farley, K.A., 2009, Apatite (U-Th)/He thermochronometry using a radiation damage accumulation and annealing model: Geochimica et Cosmochimica Acta, v. 73, p. 2347–2365, https://doi.org/10.1016/j.gca.2009.01.015.

Flowers, R.M., Farley, K.A., and Ketcham, R.A., 2015, A reporting protocol for thermochronologic modeling illustrated with data from the Grand Canyon: Earth and Planetary Science Letters, v. 432, p. 425–435, https://doi.org/10.1016/j.epsl.2015.09.053.

Forte, A.M., and Whipple, K.X., 2019, The topographic analysis kit (TAK) for TopoToolbox: Earth Surface Dynamics, v. 7, p. 87–95, https://doi.org/10.5194/esurf-7-87-2019.

Gallagher, K., Brown, R., and Johnson, C., 1998, Fission track analysis and its applications to geological problems: Annual Review of Earth and Planetary Sciences, v. 26, p. 519–572, https://doi.org/10.1146/annurev.earth.26.1.519.

Gansser, A., 1964, Geology of the Himalayas: London, UK, Interscience, 289 p.

Garzanti, E., 2019, The Himalayan foreland basin from collision onset to the present: A sedimentary-petrology perspective, *in* Treloar, P.J., and Searle M.P., eds., Himalayan Tectonics: A Modern Synthesis: Geological Society of London Special Publication, v. 483, p. 65–122, https://doi.org/10.1144/SP483.17.

Garzanti, E., Baud, A., and Mascle, G., 1987, Sedimentary record of the northward flight of India and its collision with Eurasia (Ladakh Himalaya, India): Geodinamica Acta, v. 1, p. 297–312, https://doi.org/10.1080/09853111.1987.11105147.

Gautheron, C., Barbarand, J., Ketcham, R.A., Tassan-Got, L., van der Beek, P., Pagel, M., Pinna-Jamme, R., Couffignal, F., and Fialin, M., 2013, Chemical influence on α-recoil damage annealing in apatite: Implications for (U-Th)/He dating: Chemical Geology, v. 351, p. 257–267, https://doi.org/10.1016/j.chemgeo.2013.05.027.

Gautheron, C., Djimbi, D.M., Roques, J., Balout, H., Ketcham, R.A., Simoni, E., Pik, R., Seydoux-Guillaume, A.M., and Tassan-Got, L., 2020, A multi-method, multi-scale theoretical study of He and Ne diffusion in zircon: Geochimica et Cosmochimica Acta, v. 268, p. 348–367, https://doi.org/10.1016/j.gca.2019.10.007.

Gébelin, A., Mulch, A., Teyssier, C., Jessup, M.J., Law, R.D., and Brunel, M., 2013, The Miocene elevation of Mount Everest: Geology, v. 41, p. 799–802, https://doi.org/10.1130/G34331.1.

Gérard, B., Robert, X., Grujic, D., Gautheron, C., Audin, L., Bernet, M., and Balvay, M., 2022, Zircon (U-Th)/He Closure Temperature Lower Than Apatite Thermochronometric Systems: Reconciliation of a Paradox: Minerals, v. 12, https://doi.org/10.3390/min12020145.

Gehrels, G.E., DeCelles, P.G., Ojha, T.P., and Upreti, B.N., 2006, Geologic and U-Pb geochronologic evidence for early Paleozoic tectonism in the Dadeldhura thrust sheet, far-west Nepal Himalaya: Journal of Asian Earth Sciences, v. 28, p. 385–408, https://doi.org/10.1016/j.jseaes.2005.09.012.

Gehrels, G.E., DeCelles, P.G., Ojha, T.P., and Upreti, B.N., 2006b, Geologic and U-Th-Pb geochronologic evidence for early Paleozoic tectonism in the Kathmandu thrust sheet, central Nepal Himalaya: Geological Society of America Bulletin, v. 118, p. 185–198, https://doi.org/10.1130/B25753.1.

Ginster, U., 2018, The effects of radiation damage accumulation and annealing on helium diffusion in zircon [Ph.D. thesis]: Tucson, Arizona, USA, University of Arizona, p. 73–98.

Gleadow, A.J.W., and Duddy, I.R., 1981, A natural long-term track annealing experiment for apatite: Nuclear Tracks, v. 5, p. 169–174, https://doi.org/10.1016/0191-278X(81)90039-1.

Gleadow, A.J.W., Duddy, I.R., Green, P.F., and Lovering, J.F., 1986, Confined fission track lengths in apatite: A diagnostic tool for thermal history analysis: Contributions to Mineralogy and Petrology, v. 94, p. 405–415, https://doi.org/10.1007/BF00376334.

Green, P.F., 1981, A new look at statistics in fission-track dating: Nuclear Tracks, v. 5, p. 77–86, https://doi.org/10.1016/0191-278X(81)90029-9.

Green, P.F., Duddy, I.R., Gleadow, A.J.W., Tingate, P.R., and Laslett, G.M., 1985, Fission-track annealing in apatite: Track length measurements and the form of the Arrhenius plot: Nuclear Tracks and Radiation Measurements, v. 10, p. 323–328, https://doi.org/10.1016/0735-245X(85)90121-8.

Grujic, D., Coutand, I., Bookhagen, B., Bonnet, S., Blythe, A., and Duncan, C., 2006, Climatic forcing of erosion, landscape, and tectonics in the Bhutan Himalayas: Geology, v. 34, p. 801–804, https://doi.org/10.1130/G22648.1.

Gubbels, T.L., Isacks, B., and Farrar, E., 1993, High-level surfaces, plateau uplift, and foreland development, Bolivian central Andes: Geology, v. 21, p. 695–698, https://doi.org/10.1130/0091-7613(1993)021<0695:HLSPUA>2.3.CO;2.

Guenthner, W.R., 2021, Implementation of an Alpha Damage Annealing Model for Zircon (U-Th)/He Thermochronology With Comparison to a Zircon Fission Track Annealing Model: Geochemistry, Geophysics, Geosystems, v. 22, p. 1–16, https://doi.org/10.1029/2019GC008757.

Guenthner, W.R., Reiners, P.W., Ketcham, R.A., Nasdala, L., and Giester, G., 2013, Helium diffusion in natural zircon: Radiation damage, anisotropy, and the Interpretation of zircon (U-Th)/He thermochronology: American Journal of Science, v. 313, p. 145–198, https://doi.org/10.2475/03.2013.01.

Guenthner, W.R., Reiners, P.W., and Tian, Y., 2014, Interpreting date-eU correlations in zircon (U-Th)/He datasets: A case study from the Longmen Shan, China: Earth and Planetary Science Letters, v. 403, p. 328–339, https://doi.org/10.1016/j.epsl.2014.06.050.

Guenthner, W.R., Reiners, P.W., Drake, H., and Tillberg, M., 2017, Zircon, titanite, and apatite (U-Th)/He ages and age-eU correlations from the Fennoscandian Shield, southern Sweden: Tectonics, v. 36, p. 1254–1274, https://doi.org/10.1002/2017TC004525.

Hack, J., 1973, Stream-profile analysis and stream-gradient index: Journal of Research of the U.S. Geological Survey, v. 1, p. 421–429.

Harvey, J.E., Burbank, D.W., and Bookhagen, B., 2015, Along-strike changes in Himalayan thrust geometry: Topographic and tectonic discontinuities in western Nepal: Lithosphere, v. 7, p. 511–518, https://doi.org/10.1130/L444.1.

Hayashi, T., Yamanaka, T., Hikasa, Y., Sato, M., Kuwahara, Y., and Ohno, M., 2020, Latest Pliocene Northern Hemisphere glaciation amplified by intensified Atlantic meridional overturning circulation: Communications Earth & Environment, v. 1, p. 4–5, https://doi.org/10.1038/s43247-020-00023-4.

He, D., Webb, A.A.G., Larson, K.P., and Schmitt, A.K., 2016, Extrusion vs. duplexing models of Himalayan mountain building 2: The South Tibet detachment at the Dadeldhura klippe: Tectonophysics, v. 667, p. 87–107, https://doi.org/10.1016/j.tecto.2015.11.014.

Herman, F., Seward, D., Valla, P.G., Carter, A., Kohn, B., Willett, S.D., and Ehlers, T.A., 2013, Worldwide acceleration of mountain erosion under a cooling climate: Nature, v. 504, p. 423–426, https://doi.org/10.1038/nature12877.

Hodges, K.V., 2000, Tectonics of the Himalaya and Southern Tibet from two perspectives: Geological Society of America Bulletin, v. 112, p. 324–350, https://doi.org/10.1130/0016-7606(2000)112<324:TOTHAS>2.0.CO;2.

Hodges, K.V., Parrish, R.R., and Searle, M.P., 1996, Tectonic evolution of the central Annapurna Range, Nepalese Himalayas: Tectonics, v. 15, p. 1264–1291, https://doi.org/10.1029/96TC01791.

House, M.A., Farley, K.A., and Stockli, D., 2000, Helium chronometry of apatite and titanite using Nd-YAG laser heating: Earth and Planetary Science Letters, v. 183, p. 365–368, https://doi.org/10.1016/S0012-821X(00)00286-7.

Howard, A.D., and Kerby, G., 1983, Channel changes in badlands: Geological Society of America Bulletin, v. 94, p. 739–752, https://doi.org/10.1130/0016-7606(1983)94<739:CCIB>2.0.CO;2.

Hu, X.M., Garzanti, E., An, W., and Hu, X.F., 2015, Provenance and drainage system of the Early Cretaceous volcanic detritus in the Himalaya as constrained by detrital zircon geochronology: Journal of Palaeogeography, v. 4, p. 85–98, https://doi.org/10.3724/SP.J.1261.2015.00069.

Hurford, A.J., and Green, P.D., 1983, The zeta age calibration of fission-track dating: Chemical Geology, v. 41, p. 285–317, https://doi.org/10.1016/S0009-2541(83)80026-6.

Ingalls, M., Rowley, D., Olack, G., Currie, B., Li, S., Schmidt, J., Tremblay, M., Polissar, P., Shuster, D.L., Lin, D., and Colman, A., 2018, Paleocene to Pliocene low-latitude, high-elevation basins of southern Tibet: Implications for tectonic models of India-Asia collision, Cenozoic climate, and geochemical weathering: Geological Society of America Bulletin, v. 130, p. 307–330, https://doi.org/10.1130/B31723.1.

Islam, M.N., Das, S., and Uyeda, H., 2010, Calibration of TRMM derived rainfall over Nepal during 1998–2007:

The Open Atmospheric Science Journal, v. 4, p. 12–23, https://doi.org/10.2174/1874282301004010012.

Jepson, G., Carrapa, B., Gillespie, J., Feng, R., DeCelles, P.G., Kapp, P., Tabor, C.R., and Zhu, J., 2021, Climate as the great equalizer of continental-scale erosion: Geophysical Research Letters, v. 48, no. 20, p. 1–17, https://doi.org/10.1029/2021GL095008.

Jessup, M.J., Law, R.D., Searle, M.P., and Hubbard, M.S., 2006, Structural evolution and vorticity of flow during extrusion and exhumation of the Greater Himalayan Slab, Mount Everest Massif, Tibet/Nepal: Implications for orogen-scale flow partitioning, *in* Law, R.D., Searle, M.P., and Godlin, L., eds., Channel Flow, Ductile Extrusion and Exhumation in Continental Collision Zones: Geological Society of London Special Publication, v. 268, p. 379–413, https://doi.org/10.1144/GSL.SP.2006.268.01.18.

Kapp, P., and DeCelles, P.G., 2019, Mesozoic–Cenozoic geological evolution of the Himalayan-Tibetan orogen and working tectonic hypotheses: American Journal of Science, v. 319, p. 159–254, https://doi.org/10.2475/03.2019.01.

Kennan, L., Lamb, S.H., and Hoke, L., 1997, High-altitude palaeosurfaces in the Bolivian Andes: Evidence for late Cenozoic surface uplift, *in* Widdowson, M., eds., Palaeosurfaces: Recognition, Reconstruction and Palaeoenvironmental Interpretation: Geological Society of London Special Publications, v. 120, p. 307–323, https://doi.org/10.1144/GSL.SP.1997.120.01.20.

Ketcham, R.A., 2005, Forward and inverse modeling of low-temperature thermochronometry data: Reviews in Mineralogy and Geochemistry, v. 58, p. 275–314, https://doi.org/10.2138/rmg.2005.58.11.

Ketcham, R.A., 2017, HeFTy Version 1.9.3, Manual.

Ketcham, R.A., Donelick, R.A., and Carlson, W.D., 1999, Variability of apatite fission-track annealing kinetics: II. Crystallographic orientation effects: The American Mineralogist, v. 84, p. 1235–1255, https://doi.org/10.2138/am-1999-0903.

Ketcham, R.A., Carter, A., Donelick, R.A., Barbarand, J., and Hurford, A.J., 2007, Improved modeling of fission-track annealing in apatite: The American Mineralogist, v. 92, p. 799–810, https://doi.org/10.2138/am.2007.2281.

Ketcham, R.A., Gautheron, C., and Tassan-Got, L., 2011, Accounting for long alpha-particle stopping distances in (U-Th-Sm)/He geochronology: Refinement of the baseline case: Geochimica et Cosmochimica Acta, v. 75, p. 7779–7791, https://doi.org/10.1016/j.gca.2011.10.011.

Ketcham, R.A., Guenthner, W.R., and Reiners, P.W., 2013, Geometric analysis of radiation damage connectivity in zircon, and its implications for helium diffusion: The American Mineralogist, v. 98, p. 350–360, https://doi.org/10.2138/am.2013.4249.

Kirby, E., and Whipple, K., 2001, Quantifying differential rock-uplift rates via stream profile analysis: Geology, v. 29, p. 415–418, https://doi.org/10.1130/0091-7613(2001)029<0415:QDRURV>2.0.CO;2.

Kohn, M.J., 2014, Himalayan metamorphism and its tectonic implications: Annual Review of Earth and Planetary Sciences, v. 42, p. 381–419, https://doi.org/10.1146/annurev-earth-060313-055005.

Loget, N., and Driessche, J.V.D., 2009, Wave train model for knickpoint migration: Geomorphology, v. 106, p. 376–382, https://doi.org/10.1016/j.geomorph.2008.10.017.

Long, S.P., and Robinson, D.M., 2021, Construction of the Lesser 1 Himalayan-Subhimalayan thrust belt: The primary driver of thickening, exhumation, and high elevations in the Himalayan orogen since the middle Miocene: Geology, v. 49, p. 1283–1288, https://doi.org/10.1130/G48967.1.

Mackey, B.H., Scheingross, J.S., Lamb, M.P., and Farley, K.A., 2014, Knickpoint formation, rapid propagation, and landscape response following coastal cliff retreat at the last interglacial sea-level highstand: Kaua'i, Hawai'i: Geological Society of America Bulletin, v. 126, p. 925–942, https://doi.org/10.1130/B30930.1.

Mandal, S., Robinson, D.M., Kohn, M.J., Khanal, S., and Das, O., 2019, Examining the tectono-stratigraphic architecture, structural geometry, and kinematic evolution of the Himalayan fold-thrust belt, Kumaun, northwest India: Lithosphere, v. 11, p. 414–435, https://doi.org/10.1130/L1050.1.

Masek, J.G., Isacks, B.L., Gubbels, T.L., and Fielding, E.J., 1994, Erosion and Tectonics at the margins of continental plateaus: Journal of Geophysical Research. Solid Earth, v. 99, p. 13941–13956, https://doi.org/10.1029/94JB00461.

Meesters, A.G.C.A., and Dunai, T.J., 2002, Solving the production-diffusion equation for finite diffusion domains of various shapes part I. Implications for low-temperature (U-Th)/He thermochronology: Chemical Geology, v. 186, p. 333–344, https://doi.org/10.1016/S0009-2541(01)00422-3.

Métivier, F., Gaudemer, Y., Tapponnier, P., and Klein, M., 1999, Mass accumulation rates in Asia during the Cenozoic: Geophysical Journal International, v. 137, p. 280–318, https://doi.org/10.1046/j.1365-246X.1999.00802.x.

Mitra, G., Bhattacharyya, K., and Mukul, M., 2010, The Lesser Himalayan duplex in Sikkim: Implications for variations in Himalayan shortening: Journal of the Geological Society of India, v. 75, p. 289–301, https://doi.org/10.1007/s12594-010-0016-x.

Molnar, P., Boos, W.R., and Battisti, D.S., 2010, Orographic controls on climate and paleoclimate of Asia: Thermal and mechanical roles for the Tibetan plateau: Annual Review of Earth and Planetary Sciences, v. 38, p. 77–102, https://doi.org/10.1146/annurev-earth-040809-152456.

Murphy, M. A., Yin, A., Harrison, T. M., Dürr, S. B., Chen, Z., Ryerson, F. J., Kidd, W. S. F., Wang, X., and Zhou, X., 1997, Did the Indo-Asian collision alone create the Tibetan plateau?: Geology, v. 25, p. 719–722, https://doi.org/10.1130/0091-7613(1997)025<0719:DTIACA>2.3.CO;2.

Murray, K.E., Orme, D.A., and Reiners, P.W., 2014, Effects of U-Th-rich grain boundary phases on apatite helium ages: Chemical Geology, v. 390, p. 135–151, https://doi.org/10.1016/j.chemgeo.2014.09.023.

Murrell, G.R., Sobel, E.R., Carrapa, B., and Andriessen, P., 2009, Calibration and comparison of etching techniques for apatite fission-track thermochronology, *in* Lisker, F., Ventura, B., and Glasmacher, U.A., eds., Thermochronological Methods: From Palaeotemperature Constraints to Landscape Evolution Models: Geological Society of London Special Publication, v. 324, p. 73–85, https://doi.org/10.1144/SP324.6.

Naeser, C.W., 1967, The use of apatite and sphene for fission track age determinations: Geological Society of America Bulletin, v. 78, p. 1523–1526, https://doi.org/10.1130/0016-7606(1967)78[1523:TUOAAS]2.0.CO;2.

Najman, Y., 2006, The detrital record of orogenesis: A review of approaches and techniques used in the Himalayan sedimentary basins: Earth-Science Reviews, v. 74, p. 1–72, https://doi.org/10.1016/j.earscirev.2005.04.004.

Najman, Y., and Garzanti, E., 2000, Reconstructing early Himalayan tectonic evolution and paleogeography from Tertiary foreland basin sedimentary rocks, northern India: Geological Society of America Bulletin, v. 112, p. 435–449, https://doi.org/10.1130/0016-7606(2000)112<435:REHTEA>2.0.CO;2.

Nasdala, L., Reiners, P.W., Garver, J.I., Kennedy, A.K., Stern, R.A., Balan, E., and Wirth, R., 2004, Incomplete retention of radiation damage in zircon from Sri Lanka: The American Mineralogist, v. 89, p. 219–231, https://doi.org/10.2138/am-2004-0126.

Orme, D.A., Reiners, P.W., Hourigan, J.K., and Carrapa, B., 2015, Effects of inherited cores and magmatic overgrowths on zircon (U-Th)/He ages and age-eU trends from Greater Himalayan sequence rocks, Mount Everest region, Tibet: Geochemistry, Geophysics, Geosystems, v. 16, p. 2499–2507, https://doi.org/10.1002/2015GC005818.

Orme, D.A., Guenthner, W.R., Laskowski, A.K., and Reiners, P.W., 2016, Long-term tectonothermal history of Laramide basement from zircon-He age-eU correlations: Earth and Planetary Science Letters, v. 453, p. 119–130, https://doi.org/10.1016/j.epsl.2016.07.046.

Owen, L.A., 2009, Latest Pleistocene and Holocene glacier fluctuations in the Himalaya and Tibet: Quaternary Science Reviews, v. 28, p. 2150–2164, https://doi.org/10.1016/j.quascirev.2008.10.020.

Owen, L.A., Derbyshire, E., and Fort, M., 1998, The quaternary glacial history of the Himalaya: Journal of Quaternary Science, v. 13, p. 91–120.

Pearson, O.N., and DeCelles, P.G., 2005, Structural geology and regional tectonic significance of the Ramgarh thrust, Himalayan fold-thrust belt of Nepal: Tectonics, v. 24, no. 4, https://doi.org/10.1029/2003TC001617.

Pedersen, V.K., Huismans, R.S., Herman, F., and Egholm, D.L., 2014, Controls of initial topography on temporal and spatial patterns of glacial erosion: Geomorphology, v. 223, p. 96–116, https://doi.org/10.1016/j.geomorph.2014.06.028.

Phillips, J.D., 2002, Erosion, isostatic response, and the missing peneplains: Geomorphology, v. 45, p. 225–241, https://doi.org/10.1016/S0169-555X(01)00156-8.

Quade, J., Breecker, D.O., Daëron, M., and Eiler, J., 2011, The paleoaltimetry of Tibet: An isotopic perspective: American Journal of Science, v. 311, p. 77–115, https://doi.org/10.2475/02.2011.01.

Quade, J., et al., 2020, Resetting Southern Tibet: The serious challenge of obtaining primary records of Paleoaltimetry: Global and Planetary Change, v. 191, https://doi.org/10.1016/j.gloplacha.2020.103194.

Raiverman, V., Kunte, S.V., and Mukherjea, A., 1983, Basin geometry, Cenozoic sedimentation and hydrocarbon in northwestern Himalaya and Indo-Gangetic plains: Petroleum Asia Journal, v. 6, p. 67–92.

Ravikant, V., Wu, F.Y., and Ji, W.Q., 2011, U-Pb age and Hf isotopic constraints of detrital zircons from the Himalayan foreland Subathu sub-basin on the Tertiary palaeogeography of the Himalaya: Earth and Planetary Science Letters, v. 304, p. 356–368, https://doi.org/10.1016/j.epsl.2011.02.009.

Recanati, A., Gautheron, C., Barbarand, J., Missenard, Y., Pinna-Jamme, R., Tassan-Got, L., Carter, A., Douville, E., Bordier, L., Pagel, M., and Gallagher, K., 2017, Helium trapping in apatite damage: Insights from (U-Th-Sm)/He dating of different granitoid lithologies: Chemical Geology, v. 470, p. 116–131, https://doi.org/10.1016/j.chemgeo.2017.09.002.

Reiners, P.W., 2005, Zircon (U-TH)/He thermochronometry: Reviews in Mineralogy and Geochemistry, v. 58, p. 151–179, https://doi.org/10.2138/rmg.2005.58.6.

Reiners, P.W., and Brandon, M.T., 2006, Using thermochronology to understand orogenic erosion: Annual Review of Earth and Planetary Sciences, v. 34, p. 419–466, https://doi.org/10.1146/annurev.earth.34.031405.125202.

Reiners, P.W., and Farley, K.A., 2001, Influence of crystal size on apatite (U-Th)/He thermochronology: An example from the Bighorn Mountains, Wyoming: Earth and Planetary Science Letters, v. 188, p. 413–420, https://doi.org/10.1016/S0012-821X(01)00341-7.

Reiners, P.W., and Nicolescu, S., 2006, Measurement of parent nuclides for (U-Th)/He chronometry by solution sector ICP-MS, ARHDL Report 1, http://www.geo.arizona.edu/~reiners/arhdl/arhdl.htm.

Roback, K., Clark, M.K., West, A.J., Zekkos, D., Li, G., Gallen, S.F., Chamlagain, D., and Godt, J.W., 2018, The size, distribution, and mobility of landslides caused by the 2015 Mw7.8 Gorkha earthquake, Nepal: Geomorphology, v. 301, p. 121–138, https://doi.org/10.1016/j.geomorph.2017.01.030.

Robert, X., van der Beek, P., Braun, J., Perry, C., Dubille, M., and Mugnier, J.L., 2009, Assessing quaternary reactivation of the Main Central thrust zone (central Nepal Himalaya): New thermochronologic data and numerical modeling: Geology, v. 37, p. 731–734, https://doi.org/10.1130/G25736A.1.

Robert, X., Van Der Beek, P., Braun, J., Perry, C., and Mugnier, J.L., 2011, Control of detachment geometry on lateral variations in exhumation rates in the Himalaya: Insights from low-temperature thermochronology and numerical modeling: Journal of Geophysical Research. Solid Earth, v. 116, https://doi.org/10.1029/2010JB007893.

Robinson, D.M., and Martin, A.J., 2014, Reconstructing the Greater Indian margin: Focusing on the Lesser Himalayan duplex: Tectonics, v. 33, p. 2143–2168, https://doi.org/10.1002/2014TC003564.

Robinson, D.M., DeCelles, P.G., and Copeland, P., 2006, Tectonic evolution of the Himalayan thrust belt in western Nepal: Implications for channel flow models: Geological Society of America Bulletin, v. 118, p. 865–885, https://doi.org/10.1130/B25911.1.

Robl, J., Hergarten, S., and Prasicek, G., 2020, Glacial erosion promotes high mountains on thin crust: Earth and Planetary Science Letters, v. 538, https://doi.org/10.1016/j.epsl.2020.116196.

Rohrmann, A., Kapp, P., Carrapa, B., Reiners, P.W., Guynn, J., Ding, L., and Heizler, M., 2012, Thermochronologic evidence for plateau formation in central Tibet: By 45 Ma: Geology, v. 40, p. 187–190, https://doi.org/10.1130/G32530.1.

Saha, S., Owen, L.A., Orr, E.N., and Caffee, M.W., 2019a, Cosmogenic 10Be and equilibrium-line altitude dataset of Holocene glacier advances in the Himalayan-Tibetan orogen: Data in Brief, v. 26, https://doi.org/10.1016/j.dib.2019.104412.

Saha, S., Owen, L.A., Orr, E.N., and Caffee, M.W., 2019b, High-frequency Holocene glacier fluctuations in the Himalayan-Tibetan orogen: Quaternary Science Reviews, v. 220, p. 372–400, https://doi.org/10.1016/j.quascirev.2019.07.021.

Sakai, H., Sawada, M., Takigami, Y., Orihashi, Y., Danhara, T., Iwano, H., Kuwahara, Y., Dong, Q., Cai, H., and Li, J., 2005, Geology of the summit limestone of Mount Qomolangma (Everest) and cooling history of the Yellow Band under the Qomolangma detachment: The Island Arc, v. 14, p. 297–310, https://doi.org/10.1111/j.1440-1738.2005.00499.x.

Sakai, H., Iwano, H., Danhara, T., Hirata, T., and Takigami, Y., 2013, Emplacement of hot lesser Himalayan nappes from 15 to 10 Ma in the Jumla-Surkhet region, western Nepal, and their thermal imprint on the underlying early Miocene fluvial Dumri Formation: The Island Arc, v. 22, p. 361–381, https://doi.org/10.1111/iar.12030.

Schelling, D., 1992, The tectonostratigraphy and structure of the eastern Nepal Himalaya: Tectonics, v. 11, p. 925–943, https://doi.org/10.1029/92TC00213.

Schildgen, T.F., Hodges, K.V., Whipple, P.W., Reiners, P.W., and Pringle, M.S., 2007, Uplift of the western margin of the Andean plateau revealed from canyon incision history, southern Peru: Geology, v. 35, p. 523–526, https://doi.org/10.1130/G23532A.1.

Schoenbohm, L.M., Whipple, K.X., Burchfiel, B.C., and Chen, L., 2004, Geomorphic constraints on surface uplift, exhumation, and plateau growth in the Red River region, Yunnan Province, China: Geological Society of America Bulletin, v. 116, p. 895–909, https://doi.org/10.1130/B25364.1.

Schwanghart, W., and Scherler, D., 2014, Short Communication: TopoToolbox 2 - MATLAB-based software for topographic analysis and modeling in Earth surface sciences: Earth Surface Dynamics, v. 2, p. 1–7, https://doi.org/10.5194/esurf-2-1-2014.

Searle, M.P., Windley, B.F., Coward, M.P., Cooper, D.J.W., Rex, A.J., Rex, D., Tingdong, L., Xuchang, X., Jan, M.Q., Thakur, V.C., and Kumar, S., 1987, The closing of Tethys and the tectonics of the Himalaya: Geological Society of America Bulletin, v. 98, p. 678–701, https://doi.org/10.1130/0016-7606(1987)98<678:TCOTAT>2.0.CO;2.

Searle, M.P., Simpson, R.L., Law, R.D., Parrish, R.R., and Waters, D.J., 2003, The structural geometry, metamorphic and magmatic evolution of the Everest massif, High Himalaya of Nepal-South Tibet: Journal of the Geological Society, v. 160, p. 345–366, https://doi.org/10.1144/0016-764902-126.

Shuster, D.L., and Farley, K.A., 2009, The influence of artificial radiation damage and thermal annealing on helium diffusion kinetics in apatite: Geochimica et Cosmochimica Acta, v. 73, p. 183–196, https://doi.org/10.1016/j.gca.2008.10.013.

Shuster, D.L., Flowers, R.M., and Farley, K.A., 2006, The influence of natural radiation damage on helium diffusion kinetics in apatite: Earth and Planetary Science Letters, v. 249, p. 148–161, https://doi.org/10.1016/j.epsl.2006.07.028.

Shuster, D.L., Cuffey, K.M., Sanders, J.W., and Balco, G., 2011, Thermochronometry reveals headward propagation of erosion in an alpine landscape: Science, v. 332, p. 84–88, https://doi.org/10.1126/science.1198401.

Simoes, M., Sassolas-Serrayet, T., Cattin, R., Le Roux-Mallouf, R., Ferry, M., and Drukpa, D., 2021, Topographic disequilibrium, landscape dynamics and active tectonics: An example from the Bhutan Himalaya: Earth Surface Dynamics, v. 9, p. 895–921, https://doi.org/10.5194/esurf-9-895-2021.

Soucy La Roche, R.S., Godin, L., Cottle, J.M., and Kellett, D.A., 2016, Direct shear fabric dating constrains early Oligocene onset of the South Tibetan detachment in the western Nepal Himalaya: Geology, v. 44, p. 403–406, https://doi.org/10.1130/G37754.1.

Soucy La Roche, R.S., Godin, L., Cottle, J.M., and Kellett, D.A., 2018a, Preservation of the early evolution of the Himalayan middle crust in foreland klippen: Insights from the Karnali Klippe, west Nepal: Tectonics, v. 37, p. 1161–1193, https://doi.org/10.1002/2017TC004847.

Soucy La Roche, R.S., Godin, L., and Crowley, J.L., 2018b, Reappraisal of emplacement models for Himalayan external crystalline nappes: The Jajarkot klippe, western Nepal: Geological Society of America Bulletin, v. 130, p. 1041–1056, https://doi.org/10.1130/B31799.1.

Spiegel, C., Kohn, B., Belton, D., Berner, Z., and Gleadow, A., 2009, Apatite (U-Th-Sm)/He thermochronology of rapidly cooled samples: The effect of He implantation: Earth and Planetary Science Letters, v. 285, p. 105–114, https://doi.org/10.1016/j.epsl.2009.05.045.

Srivastava, P., and Mitra, G., 1994, Thrust geometries and deep structure of the outer and lesser Himalaya, Kumaon and Garhwal (India): Implications for evolution of the Himalayan fold-and-thrust belt: Tectonics, v. 13, p. 89–109, https://doi.org/10.1029/93TC01130.

Stevens Goddard, A.L., Larrovere, M.A., Carrapa, B., Aciar, R.H., and Alvarado, P., 2018, Reconstructing the thermal and exhumation history of the Sierras Pampeanas through low-temperature thermochronology: A case study from the Sierra de Velasco: Geological Society of America Bulletin, v. 130, p. 1842–1858, https://doi.org/10.1130/B31935.1.

Streule, M.J., Carter, A., Searle, M.P., and Cottle, J.M., 2012, Constraints on brittle field exhumation of the Everest-Makalu section of the Greater Himalayan Sequence: Implications for models of crustal flow: Tectonics, v. 31, no. 3, https://doi.org/10.1029/2011TC003062.

Szulc, A.G., et al., 2006, Tectonic evolution of the Himalaya constrained by detrital ^{40}Ar-^{39}Ar, Sm-Nd and petrographic data from the Siwalik foreland basin succession, SW Nepal: Basin Research, v. 18, p. 375–391, https://doi.org/10.1111/j.1365-2117.2006.00307.x.

Thiede, R.C., and Ehlers, T.A., 2013, Large spatial and temporal variations in Himalayan denudation: Earth and Planetary Science Letters, v. 371–372, p. 278–293, https://doi.org/10.1016/j.epsl.2013.03.004.

Tokuoka, T., Takayasu, K., Yoshida, M., and Hisatomi, K., 1986, The Churia (Siwalik) Group of the Arung Khola area, west central Nepal: Memoirs of the Faculty of Science: Shimane University, v. 20, p. 135–210.

Uddin, A., and Lundberg, N., 1998, Cenozoic history of the Himalayan-Bengal system: Sand composition in the Bengal basin, Bangladesh: Geological Society of America Bulletin, v. 110, p. 497–511, https://doi.org/10.1130/0016-7606(1998)110<0497:CHOTHB>2.3.CO;2.

Valdiya, K.S., 1980, Geology of Kumaun Lesser Himalaya: Dehra Dun, India, Institute of Himalayan Geology, 291 p.

van der Beek, P., Van Melle, J., Guillot, S., Pcher, A., Reiners, P.W., Nicolescu, S., and Latif, M., 2009, Eocene Tibetan plateau remnants preserved in the northwest Himalaya: Nature Geoscience, v. 2, p. 364–368, https://doi.org/10.1038/ngeo503.

van der Beek, P., Litty, C., Baudin, M., Mercier, J., Robert, X., and Hardwick, E., 2016, Contrasting tectonically driven exhumation and incision patterns, western versus central Nepal Himalaya: Geology, v. 44, p. 327–330, https://doi.org/10.1130/G37579.1.

Vermeesch, P., 2010, HelioPlot, and the treatment of overdispersed (U-Th-Sm)/He data: Chemical Geology, v. 271, p. 108–111, https://doi.org/10.1016/j.chemgeo.2010.01.002.

Vermeesch, P., and Tian, Y., 2014, Thermal history modelling: HeFTy vs. QTQt: Earth-Science Reviews, v. 139, p. 279–290, https://doi.org/10.1016/j.earscirev.2014.09.010.

Wang, A., Garver, J.I., Wang, C., Smith, J.A., and Zhang, K., 2010, Episodic exhumation of the Greater Himalayan Sequence since the Miocene constrained by fission track thermochronology in Nyalam, central Himalaya: Tectonophysics, v. 495, p. 315–323, https://doi.org/10.1016/j.tecto.2010.09.037.

Warnock, A.C., Zeitler, P.K., Wolf, R.A., and Bergman, S.C., 1997, An evaluation of low-temperature apatite U-Th/He thermochronometry: Geochimica et Cosmochimica Acta, v. 61, p. 5371–5377, https://doi.org/10.1016/S0016-7037(97)00302-5.

Whipple, K.X., DiBiase, R.A., Ouimet, W.B., and Forte, A.M., 2017a, Preservation or piracy: Diagnosing low-relief, high-elevation surface formation mechanisms: Geology, v. 45, p. 91–94, https://doi.org/10.1130/G38490.1.

Whipple, K.X., Forte, A.M., DiBiase, R.A., Gasparini, N.M., and Ouimet, W.B., 2017b, Timescales of landscape response to divide migration and drainage capture: Implications for the role of divide mobility in landscape evolution: Journal of Geophysical Research. Earth Surface, v. 122, https://doi.org/10.1002/2016JF003973.

Widdowson, M., 1997, The geomorphological and geological importance of paleosurfaces, *in* Widdowson, M., ed., Palaeosurfaces: Recognition, Reconstruction and Palaeoenvironmental Interpretation: Geological Society of London, Special Publications, v. 120, p. 1–12, https://doi.org/10.1144/GSL.SP.1997.120.01.01.

Wilke, F.D.H., Sobel, E.R., O'Brien, P.J., and Stockli, D.F., 2012, Apatite fission track and (U-Th)/He ages from the Higher Himalayan Crystallines, Kaghan Valley, Pakistan: Implications for an Eocene Plateau and Oligocene to Pliocene exhumation: Journal of Asian Earth Sciences, v. 59, p. 14–23, https://doi.org/10.1016/j.jseaes.2012.06.014.

Willett, S., 2017, Preservation or piracy: Diagnosing low-relief, high-elevation surface formation mechanisms: COMMENT: Geology, v. 45, no. 8, e421, https://doi.org/10.1130/G38929C.1.

Willett, S.D., Mccoy, S.W., Perron, J.T., Goren, L., and Chen, C., 2014, Dynamic reorganization of river basins: Science, v. 343, https://doi.org/10.1126/science.1248765.

Winn, C., Karlstrom, K.E., Shuster, D.L., Kelley, S., and Fox, M., 2017, 6 Ma age of carving Westernmost Grand Canyon: Reconciling geologic data with combined AFT, (U-Th)/He, and $^{4}He/^{3}He$ thermochronologic data: Earth and Planetary Science Letters, v. 474, p. 257–271, https://doi.org/10.1016/j.epsl.2017.06.051.

Wolf, R.A., Farley, K.A., and Silver, L.T., 1996, Helium diffusion and low-temperature thermochronometry of apatite: Geochimica et Cosmochimica Acta, v. 60, p. 4231–4240, https://doi.org/10.1016/S0016-7037(96)00192-5.

Yang, R., Willett, S.D., and Goren, L., 2015, In situ low-relief landscape formation as a result of river network disruption: Nature, v. 520, p. 526–529, https://doi.org/10.1038/nature14354.

Yin, A., 2006, Cenozoic tectonic evolution of the Himalayan orogen as constrained by along-strike variation of structural geometry, exhumation history, and foreland sedimentation: Earth-Science Reviews, v. 76, p. 1–131, https://doi.org/10.1016/j.earscirev.2005.05.004.

Yin, A., and Harrison, T.M., 2000, Geologic evolution of the Himalayan-Tibetan orogen: Annual Review of Earth and Planetary Sciences, v. 28, p. 211–280, https://doi.org/10.1146/annurev.earth.28.1.211.

Zapata, S., Sobel, E.R., del Papa, C., Jelinek, A.R., and Glodny, J., 2019, Using a paleosurface to constrain low-temperature thermochronological data: Tectonic evolution of the Cuevas Range, central Andes: Tectonics, v. 38, p. 3939–3958, https://doi.org/10.1029/2019TC005887.

Zeitler, P.K., Herczeg, A.L., McDougall, I., and Honda, M., 1987, U-Th-He dating of apatite: A potential thermochronometer: Geochimica et Cosmochimica Acta, v. 51, p. 2865–2868, https://doi.org/10.1016/0016-7037(87)90164-5.

Zhang, H., Oskin, M.E., Liu-Zeng, J., Zhang, P., Reiners, P.W., and Xiao, P., 2016, Pulsed exhumation of interior eastern Tibet: Implications for relief generation mechanisms and the origin of high-elevation planation surfaces: Earth and Planetary Science Letters, v. 449, p. 176–185, https://doi.org/10.1016/j.epsl.2016.05.048.

Science Editor: Brad Singer
Associate Editor: William Guenthner

Manuscript Received 9 February 2022
Revised Manuscript Received 17 May 2022
Manuscript Accepted 4 September 2022

Printed in the USA